January 2015

Analysis and Simulation of Nonlinearities in Noise Attenuation Model for a Diesel Engine Block

Jiajun Cao
Purdue University

Graduate School Form 30
Updated 1/15/2015

PURDUE UNIVERSITY
GRADUATE SCHOOL
Thesis/Dissertation Acceptance

This is to certify that the thesis/dissertation prepared

By Jiajun Cao

Entitled

ANALYSIS AND SIMULATION OF NONLINEARITIES IN NOISE ATTENUATION MODEL FOR A DIESEL ENGINE BLOCK

For the degree of Master of Science in Mechanical Engineering

Is approved by the final examining committee:

Peter H. Meckl
Chair

J. Stuart Bolton

Gregory M. Shaver

To the best of my knowledge and as understood by the student in the Thesis/Dissertation Agreement, Publication Delay, and Certification Disclaimer (Graduate School Form 32), this thesis/dissertation adheres to the provisions of Purdue University's "Policy of Integrity in Research" and the use of copyright material.

Approved by Major Professor(s): Peter H. Meckl

Approved by: Anil K. Bajaj / James D. Jones 7/8/2015

Head of the Departmental Graduate Program Date

ANALYSIS AND SIMULATION OF NONLINEARITIES IN NOISE ATTENUATION MODEL FOR A DIESEL ENGINE BLOCK

A Thesis

Submitted to the Faculty

of

Purdue University

by

Jiajun Cao

In Partial Fulfillment of the

Requirements for the Degree

of

Master of Science in Mechanical Engineering

August 2015

Purdue University

West Lafayette, Indiana

ACKNOWLEDGMENTS

I would like to express my deepest gratitude to Dr. Peter H. Meckl, my major professor and research supervisor, for providing me with the opportunity to work on this project, and for his invaluable guidance and support during my entire stay at Purdue University. His insight and enthusiasm were priceless in my understanding of the topic and completion of this thesis.

I would also like to thank Dr. J. Stuart Bolton and Dr. Gregory M. Shaver for their generous inputs as my advisory committee members. Special thanks are due to Dr. J. Stuart Bolton for his valuable advice and support on acoustic measurements.

My sincere thanks are due to Robert Brown in the technical shop at Herrick Laboratories, for his great support in fixing and maintaining the engine setup for my project. I wish to express my great appreciation to Bert Gramelspacher in the electronic shop for design and rebuild of the driver unit for fuel injectors. I would also like to extend my thanks to Ronald Evans, David Meyer and Kwok Lee at Herrick for their help during various stages of putting the engine back to work.

I wish to acknowledge, in particular, the precious help and valuable input from Jinpu Yang and Chaitanya Shankar Bhat, previous students working on this project. I also wish to thank Seungkyu Lee, a PhD student at Herrick, for his help and advice in preparation for acoustic measurements.

I would like to thank US Army Power Generation Branch for initial funding of this project. I would also like to thank Scheid Diesel Services and Bosch for their help and support on rebuilding the injectors.

Finally, I wish to thank my parents for their support in my pursuit of graduate study at Purdue, without which this work could not have been completed in the first place.

TABLE OF CONTENTS

LIST OF TABLES

LIST OF FIGURES

Figure Page

ABSTRACT

Cao, Jiajun M.S.M.E., Purdue University, August 2015. Analysis and Simulation of Nonlinearities in Noise Attenuation Model for a Diesel Engine Block. Major Professor: Dr. Peter H. Meckl, School of Mechanical Engineering.

The purpose of this thesis is to understand the characteristics of noise attenuation of a diesel engine block, by means of setting up a structural attenuation model and exploring the impact of variations of the model, in terms of nonlinearities. A model motivated by a set of experimentally-determined attenuation measurements was constructed, validated and explored for the potential for sound power prediction, with the aid of simulation.

Attenuation curves have long been considered an effective and straightforward method to understand the relationship between cylinder pressure and the corresponding noise radiation from an engine block. Preliminary measurements on a small single-cylinder diesel engine, however, suggest dependency of attenuation curves on injection parameters and operating conditions of the engine. Such dependency signals a possibility of inherent nonlinearities in the engine block attenuation and calls for a deeper investigation of the hypothesis.

A mass-spring-damper-based model was developed from the averaged experimental attenuation measurements and served as an alternative to attenuation curves to represent the noise attenuation characteristics of the engine block. The hypothesis of inherent nonlinearities was tested with the model and simulation results demonstrated relevance of nonlinearities to several off-linear behaviors of experimentally-determined attenuation curves. Validation for the model was performed by simulation under different operating conditions, and consistent observations further justified the nonlinear hypothesis. Nonlinearities were also categorized to account for different behaviors of the attenuation model.

Based on the model developed, sound power levels were predicted for a given set of cylinder pressures under different operating conditions. The simulation-model-based predictions demonstrated more reliability compared to the attenuation-curves-based prediction. Predictions among different models, linear or nonlinear, were compared and the impact of nonlinearities was analyzed. Judging the validity and accuracy of the predictions, however, requires further experimental measurements in the future.

CHAPTER 1. INTRODUCTION

Diesel engines are widely used in industry due to their high thermal efficiency and potential for increased power output when compared with other internal combustion engines such as gasoline engines. Unlike gasoline engines, where combustion starts with the ignition of air-fuel mixture by a spark, diesel engines feature compression-ignited combustion, where air is compressed in cylinder so greatly that the temperature exceeds the ignition point of fuel and subsequent fuel injection starts the combustion process. Such design requires a very high compression ratio, which leads to the most notable advantage of diesel engines – increased thermal efficiency. While a high compression ratio does increase efficiency and fuel economy, the great variations of pressure in the combustion chamber also bring a significant amount of noise. Many studies and analyses have been performed on identifying the sources of noise and in particular the correlation between the combustion process and combustion-induced noise. This thesis mainly focuses on the study of the relationship between cylinder pressure, which gives a quantitative description of the combustion process, and the radiated noise pressure level from the engine.

1.1 Motivation

The relationship between cylinder pressure and radiated noise level is considered as a structural attenuation from the engine block, as illustrated in Figure 1.1. It is a characteristic of the engine block and is independent of operating conditions such as engine speed, applied load and injection strategies. With a reasonable model, it is possible to predict noise level under certain operating conditions based on the cylinder pressure measured.

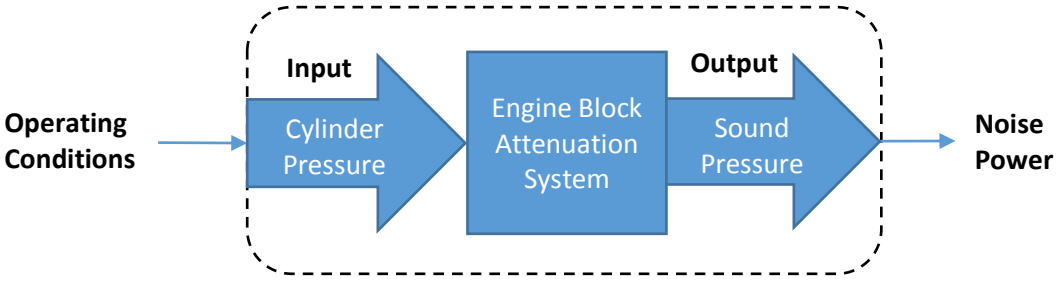

Figure 1.1. Representative Noise Attenuation System of an Engine Block.

Previous studies mainly adopted a linear approach to understand the attenuation and represented the system with an attenuation curve computed from the differences of spectra of cylinder pressure and radiated noise pressure level. Ideally, the attenuation curve is unique for a particular engine and independent of operating conditions, if the linear assumption holds true. Consequently, with the help of the one and only attenuation curve, noise pressure can be readily predicted under any circumstances provided that the corresponding cylinder pressure measurements are available.

In an attempt to predict and control noise radiation, a 3kW Tactical Quiet Generator (TQG) MEP 831A with a Yanmar L70-AE DEG FRYC 296cc single-cylinder, naturally-aspirated direct-injection engine was used for experimental study. During the earlier stage of the project, the fuel injection system, originally mechanical with fixed injection timing at 17.0 ± 1 BTDC, was replaced with electronic injection with dSPACE DS1103 as the Engine Control Unit (ECU) to provide the capability of controlling injection parameters, thus varying cylinder pressure [1]. Measurements of cylinder pressure and corresponding sound pressure of noise radiation were then conducted [2], with various injection timings and different speeds and loads, to compute the attenuation curve for the engine block. The preliminary results, however, demonstrated the dependency of attenuation curve on injection parameters (Figure 1.2). The differences between attenuation curves generated under different conditions can be as large as 10 dB, and hence multiple attenuation curves, instead of one, are needed to accurately describe the engine block attenuation system. A possible explanation for these results is that the engine block attenuation system is essentially nonlinear, which also means the attenuation curve might not be the best choice to model the system. As a result, a nonlinear model is proposed in this thesis to analyze the hypothesis of inherent nonlinearities and to better understand the engine block attenuation.

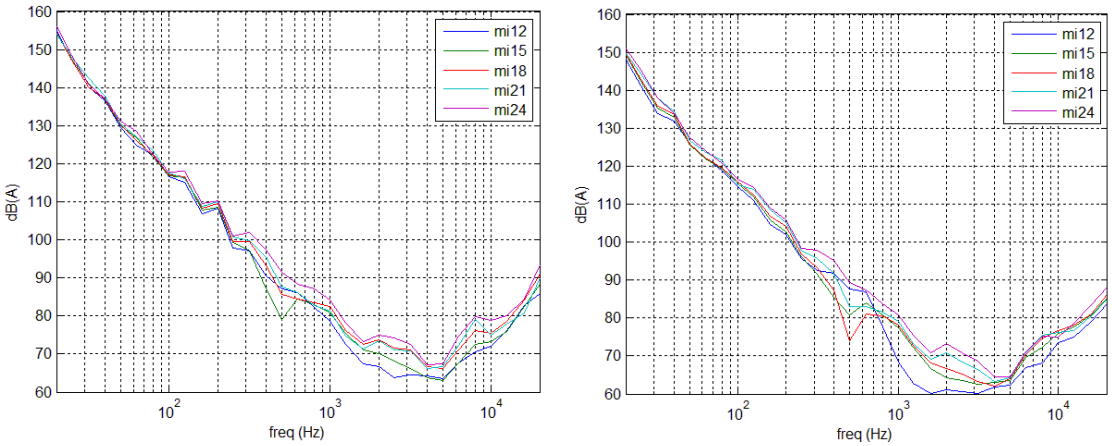

Figure 1.2. Attenuation Curves with Various Single Pulse Injection Timings for a Diesel Engine at Idle (left) and Full Load (right): “mi” stands for main injection, and the number that follows stands for advanced crank angle to top dead center when injection takes place, e.g. “mi12” stands for a single pulse injection, which is naturally the main injection pulse, at 12° crank angle before top dead center [2].

1.2 Objectives

This study mainly focuses on a nonlinear structural attenuation model modified from a traditional linear approach for a single-cylinder diesel engine. This thesis started from the experimental cylinder pressure and noise radiation data collected by the previous researcher [2], as well as the corresponding attenuation curves, generated a data-driven model for simulation and added in different kinds of nonlinearities to understand the attenuation system. The study aims to identify the nature of possible nonlinearities in the engine block attenuation system, as well as to explore the potential for prediction of noise level based on the model proposed with only cylinder pressure measurements.

1.3 Organization

This thesis is divided into six chapters. Chapter 1 provides the motivation and general background of this study as well as main objectives and a quick overview of the whole thesis. Chapter 2 focuses on more details of the background of the topic and a literature review of relative and important concepts and results shared by other previous researchers in the area. This includes an overview of diesel engines and electronic injection systems, and analysis of noise from diesel engines. Chapter 3 provides a description of the hardware setup on which the measurements used in this thesis were recorded, including an introduction to the generator and the engine, its modified electronic injection system and control unit, and the procedures for acoustic measurements. Chapter 4 focuses on the engine block structural attenuation model, proposes a model and explores the impact of adding nonlinearities. Different kinds of nonlinearities are discussed and the simulation results are compared with the experimental measurements. Several models are generated and validated through predictions of attenuation under different operating conditions. Chapter 5 explores the potential for using the simulated attenuation model to predict sound power radiation from the engine and the influence of nonlinearities on predictions. Finally, Chapter 6 serves as a summary of the work included in this thesis and provides recommendations for future work.

CHAPTER 2. BACKGROUND AND LITERATURE REVIEW

2.1 Electronic Diesel Injection Systems

Conventional diesel engines use mechanical injection systems where the fuel injection is driven by the engine crankshaft. During the compression stroke, the high-pressure pump, which delivers fuel into the injectors, is triggered at some predetermined crank angles in advance of top dead center (TDC). The high-pressure fuel then pushes open the injector and is injected into the combustion chamber. Such design ensures precise and consistent timing of start and duration of injection for each combustion cycle. However, research results show that the injection timing plays a vital role in fuel economy and emissions and consequently calls for a variable and controllable injection. An electronic injection system, where an electromagnetic solenoid actuator controls injection and encoders on the engine crankshaft return real-time crank angle readings, provides the capability for researchers and engineers to vary injection strategies and optimize the performance including efficiency and emissions.

Although electronic injection systems have already been widely used in gasoline engines in the 1980's, the progress of development of electronic diesel injection was relatively slow, mainly due to failure of early electromechanical systems to meet the requirements of high pressure and precise injection in D.I. diesel engines. The development of the diesel injection system started from only adopting electronic sensors and actuators while keeping all basic hydro-mechanical elements, to digital jerk-pump-based injection and finally progressed to modern common-rail-based electronic injection system [3]. Apart from that, modern engines are also equipped with digital sensors to measure air flows, combustion chamber pressure, temperature, exhaust emissions and other quantities that indicate the performance of engines. Such measurements, when combined with electronic injection systems, can be built into engine management and control systems where performance issues such as cold start, fuel consumption, chemical and acoustic emissions can be optimized.

2.2 Noise from Diesel Engines

Diesel engines bring bigger problems when it comes to acoustical emission due to greater pressure variations when compared with gasoline engines. Whether the engines are for on-road purposes such as in trucks and trailers, or for non-road applications such as in backhoes or generators, the noise is generally undesirable not only because it causes discomfort for the operators but also because it violates laws and regulations which get stricter every year. Table 2.1 shows representative regulations on outdoor noise levels.

Table 2.1. Representative Outdoor Noise Level Regulations [4].

Noise Zones:	Peak Daytime db(A)	Peak Nighttime db(A)	Continuous Daytime db(A)	Continuous Nighttime db(A)
Urban – Residential	62	52	57	47
Suburban – Residential	57	47	52	42
Very Quiet Suburban or Rural Residential	52	42	47	37
Urban – Nearby Industry	67	57	62	52
Heavy Industry	72	62	67	57

2.2.1 Sources of Noise from Diesel Engines

Before making any attempt to reduce the noise radiated from engines, it is important to identify the sources of noise first. Noise from diesel engines is caused by vibration of surfaces of structures, attached accessories and covers. Such vibration is mainly attributed to two basic forces: combustion forces resulting from variation of cylinder pressure in the combustion chamber and mechanical forces from engine mechanisms such as crankshaft, gear trains and pistons [5]. Austen [6] in his work identified 6 sources of noise from diesel engines:

1) Fuel Injection Equipment: The noise from injection equipment is low in intensity compared with engine noise but more observable at low engine speed and on small engines.
2) Pump Noise: The noise intensity depends greatly on mounting. A rigid mounting of pumps and flywheel, if there is any, keeps such noise negligible compared to noise from other sources.
3) Injector Noise: The noise mainly comes from the nozzle spring surge and the impact of nozzle needle with the seat on closing. Both sources can be significantly reduced by minimizing the needle mass and spring force. With a proper design, the injector noise could be negligible.
4) Engine Covers: This is a major source of noise including noises from valve cover and timing cover. It is possible to reduce such noise by replacing light cast aluminum covers with heavier steel covers reinforced with rubber or asbestos wool.

5) Flywheel and Front Pulley: The noise could be radiated at high frequencies but the noise from the flywheel, which is significant, will only be a problem if the engine is tested without a clutch housing.
6) Basic Engine Noise: This is the noise resulting from cylinder pressure variations, which in turn excites other sources of noise mentioned previously. The noise is radiated from the main surfaces of the engine structure, often the most significant and directly related to the combustion process. Since the combustion process also plays an important role in other performance attributes of engines, the basic engine noise is of most interest to researchers and also the focus of this thesis.

2.2.2 Combustion-Induced Noise

Noise from vibrations caused by mechanical forces is generally negligible or independent of operating conditions of engines. Acoustical insulation is often applied to reduce such noise. Combustion-induced noise, or the basic engine noise discussed in the previous section, is a major contributor of the overall acoustical emission and is directly dependent on operating conditions such as speed, load and injection strategies. Such noise sources not only include those directly from the vibrations of the engine main structure due to variations of cylinder pressure, but also those from vibrations of any other components and accessories because of excitation of the combustion forces and sometimes even coupled with the mechanical forces.

Engine noise can certainly be reduced by conventional acoustical methods including acoustic barriers, acoustic insulation, isolation mounts, and exhaust silencers, maximizing distance and even placing the whole engine in a sound-attenuating enclosure [6]. However, study of the correlation between noise and combustion helps understand the nature and components of noise radiated, which gives guidelines in noise reduction strategies, and also shows the potential to reduce noise from the source.

Ricardo [7-8] in the 1930's first recognized the relationship between engine noise and rapidity of combustion and detonation, and described it as "explosion strikes the walls of the cylinder with a hammer blow". The rapidity of combustion and detonation is perfectly described by cylinder pressure and many studies followed to find the correlation between cylinder pressure and noise from the engine. The shape of the cylinder pressure curve was analyzed, and criteria were generated to describe it [9]:

1) Peak cylinder pressure
2) Rate of pressure rise
3) Acceleration of pressure rise

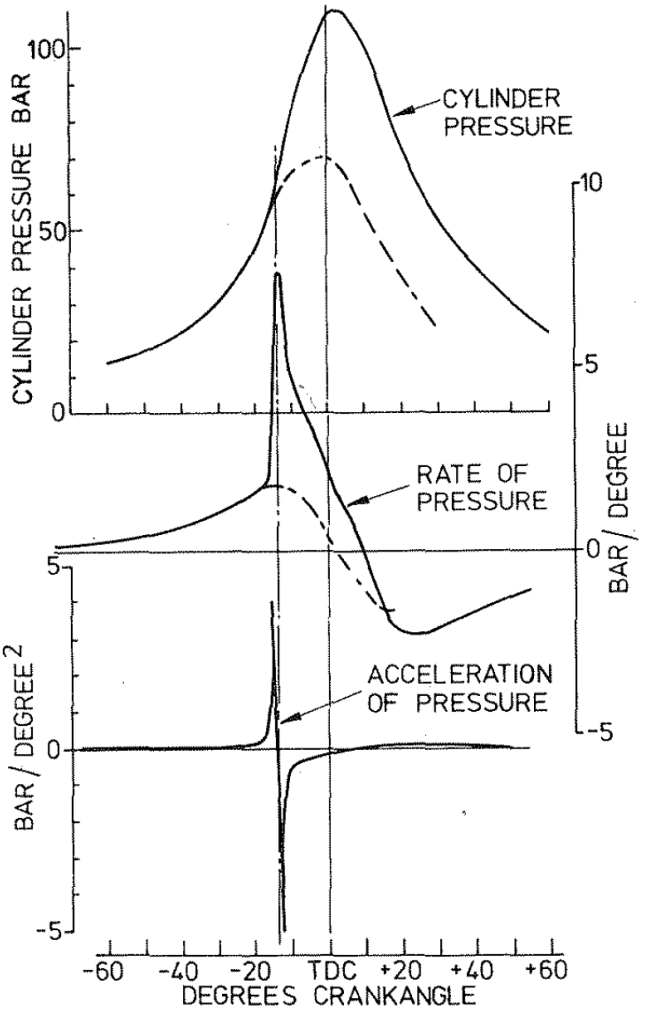

Figure 2.1. Cylinder Pressure, rate of pressure rise and acceleration of pressure rise of a high performance diesel engine [9].

Many early investigators tried to understand the combustion-induced noise, both theoretically and experimentally, based on these three criteria. Some argue the rate of pressure rise is a good indicator of noise level, some argue the acceleration to be a decisive factor while the others argue the peak cylinder pressure and the duration it lasts predominates the noise intensity. In the 1940's, Withrow, Fry and Stone [10-11] drew a very important conclusion that the correlation between the shape of cylinder pressure only exists at low engine speeds while at high speeds it is the peak cylinder pressure that is dominant. It shows that investigation with only one of the three criteria is incomplete, and due to the complexity of looking at all three criteria at the same time, another approach is needed to analyze the cylinder pressure.

Thanks to the development of spectrum analysis, researchers started to look at the cylinder pressure in the frequency domain where the information from all three criteria is included. Priede [12] in 1956 plotted the cylinder pressure spectra from a D.I. diesel engine with different injection timings (Figure 2.2), marking the start of investigation of cylinder pressure and noise

level spectrum. The differences of the cylinder pressure level spectrum and noise level spectrum are considered a characteristic of the sound-attenuation of the engine block and defined as the attenuation curve.

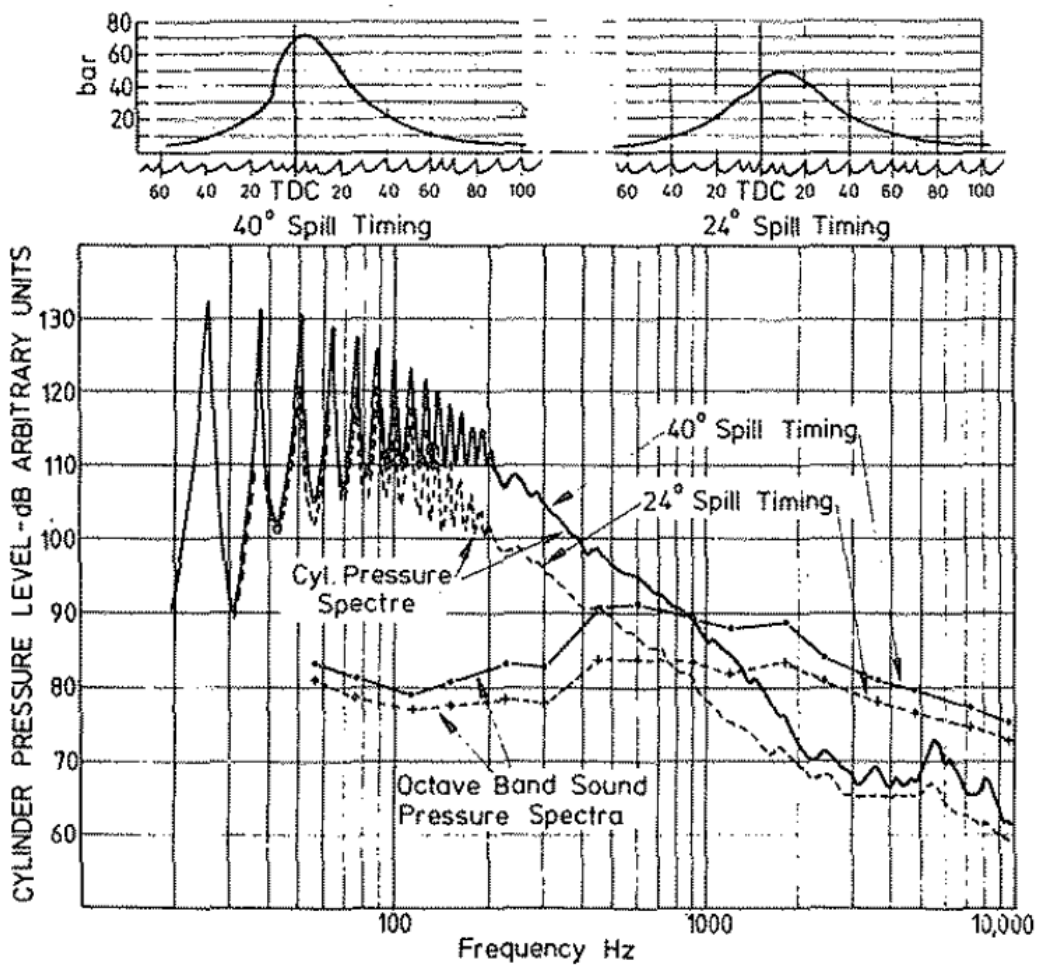

Figure 2.2. Cylinder pressure diagrams and spectra, noise spectra of a D.I. diesel engine at 1000 rpm full load [12].

2.2.3 Structural Attenuation from Engine Block

The structural attenuation is an attenuation spectrum curve and is expected to be independent of operating conditions such as speeds, loads and injection strategies. The concept, which fully describes the acoustical characteristic of an engine block, was proposed by Austen and Priede in 1958 [13]:

$$\text{Attenuation (dB)} = \text{cylinder pressure (dB)} - \text{sound pressure level (dB)} \qquad (2.1)$$

Figure 2.3 shows the attenuation curve estimated by Austen and Priede for a diesel engine, which demonstrates independency of operating conditions. Such linear attenuation model is

easy to compute and gives a good measure of sound-attenuating capability of the engine block or any enclosures it is placed within. Anderton [14] and Desantes [15] also generated attenuation curves based on this linear model (Figure 2.4).

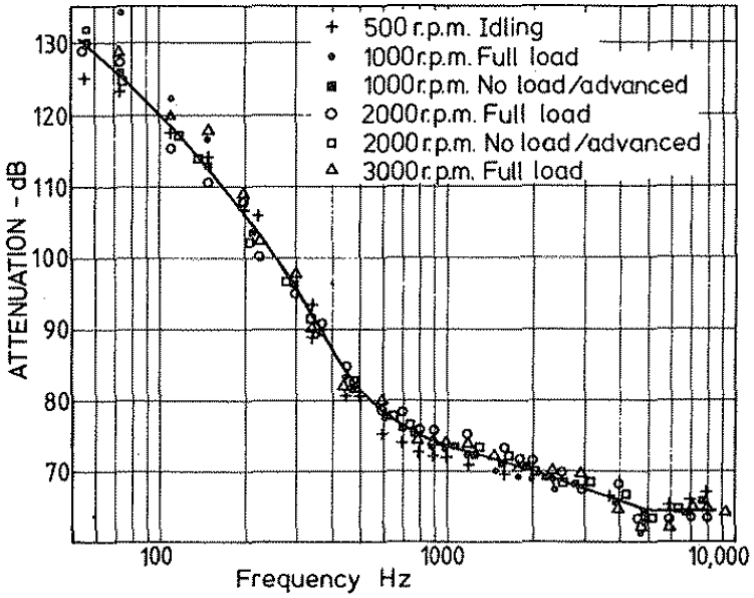

Figure 2.3. Structural and acoustical attenuation of a diesel engine [13].

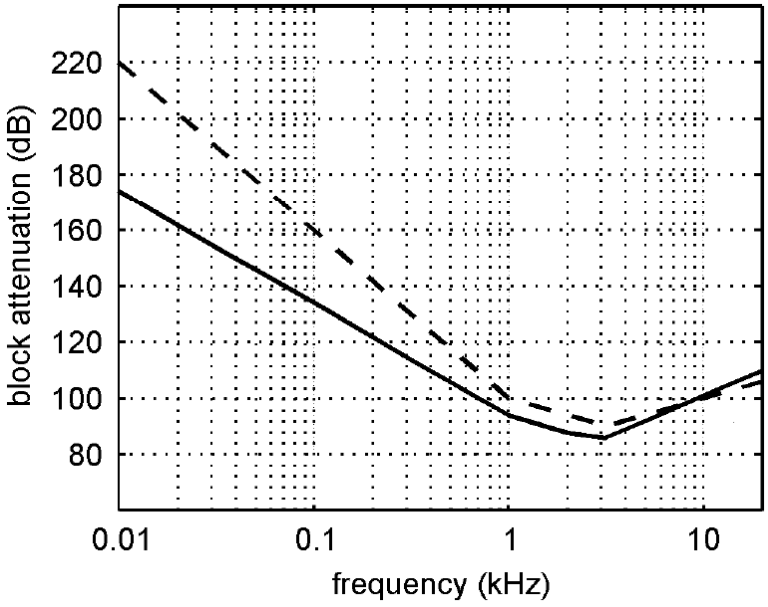

Figure 2.4. Block attenuation curve: estimated in [15] (-) and proposed in [14] (--).

This technique, however, doesn't work in all cases and Priede later showed that on engines with smooth cylinder pressure profiles, considerable discrepancies and inaccuracies were observed [16]. He first explained that the mechanical-induced noise needs to be separated in order to

achieve a linear relationship between pure combustion-induced noise and cylinder pressure level. However he later realized the mechanical-induced noise is coupled with cylinder pressure and could be possibly increased as cylinder pressure level increases. In order to isolate combustion-induced noise, more sophisticated design was added to the test [9].

CHAPTER 3. EXPERIMENTAL SETUP

The subject studied for noise attenuation is a Tactical Quiet Generator (TQG) MEP 831A with 3kW rated power. The generator is powered by a Yanmar L70-AE DEG FRYC 296cc single cylinder diesel engine. As a small engine, it was originally equipped with mechanical injection system and speed governors. In order to provide flexibility of injection strategies and study the relation between injection parameters and noise level, an electronic common-rail-based injection system was developed in the previous phase of the project [1].

3.1 Common-Rail-Based Electronic Injection System

Instead of low-pressure pumps delivering fuel to each injector, a high-pressure fuel rail is used for all injectors with solenoid valves to control fuel delivery. The rail is named as “common” because it generates the same pressure and serves as the same source of fuel to all injectors on an engine. Figure 3.1 illustrates a typical common-rail-based electronic fuel injection system. The fuel is filtered first and then pumped to high pressure and subsequently delivered to the common rail. A pressure-limiting valve and rail pressure sensor are mounted on the fuel rail. The pressure-limiting valve is usually designed as an electronic regulator, which opens up when the rail pressure exceeds the limit pre-determined by electric signals, resulting in the excessive fuel returning back to the fuel tank. The rail pressure is then roughly maintained at some certain level. However, for a more precise control of rail pressure, a rail pressure sensor needs to be incorporated. Along with the electronic control unit (ECU), which processes signal and control algorithms, a closed-loop control of rail pressure can be realized.

One of the major advantages of common-rail injection is that it allows for multiple injection strategies. As opposed to single injection, multiple injection may include pilot injection, which reduces noise level, main injection and post injection, which reduces exhaust emissions. Consequently, injection strategies are more flexible since not only main injection timing but also pilot/post injection quantity and delays between multiple injections can be varied.

Since the subject in this thesis is a single-cylinder engine, only one injector is connected to the common rail. The other outlets of the rail are plugged and rail pressure sensor and pressure regulator are still incorporated to control and maintain the rail pressure.

The injector used in this project is Bosch CRIN3 and the solenoid current trace is illustrated in Figure 3.2. The energizing time (ET) is a variable to control the duration of the opening of the solenoid valve of the injector. With the current rail pressure reading and fuel quantity, which is readily available on the fuel map, the appropriate energizing time can be estimated.

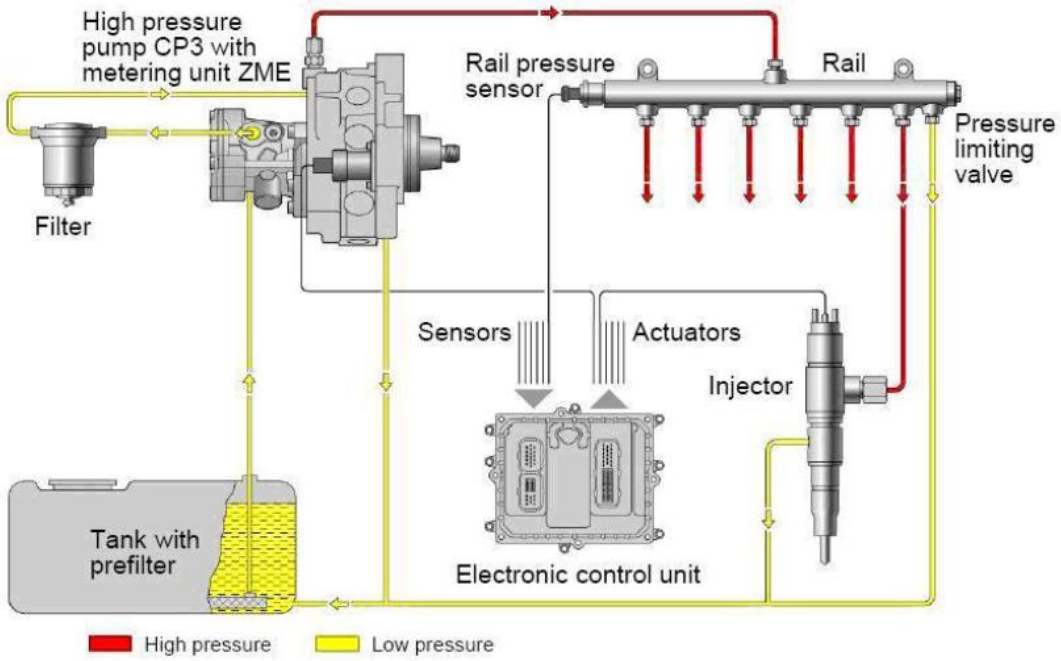

Figure 3.1. Schematic of a Bosch Common-rail Fuel Injection System [17].

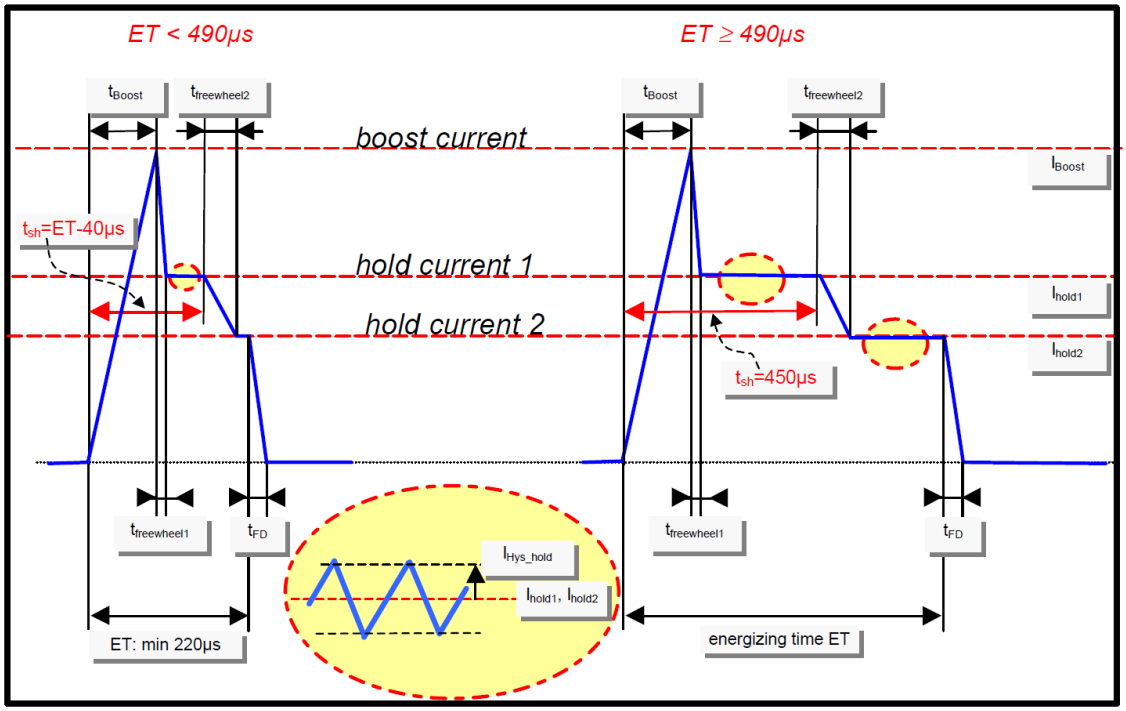

Figure 3.2. Solenoid Current Trace for CRIN3 Injector (Courtesy: Bosch).

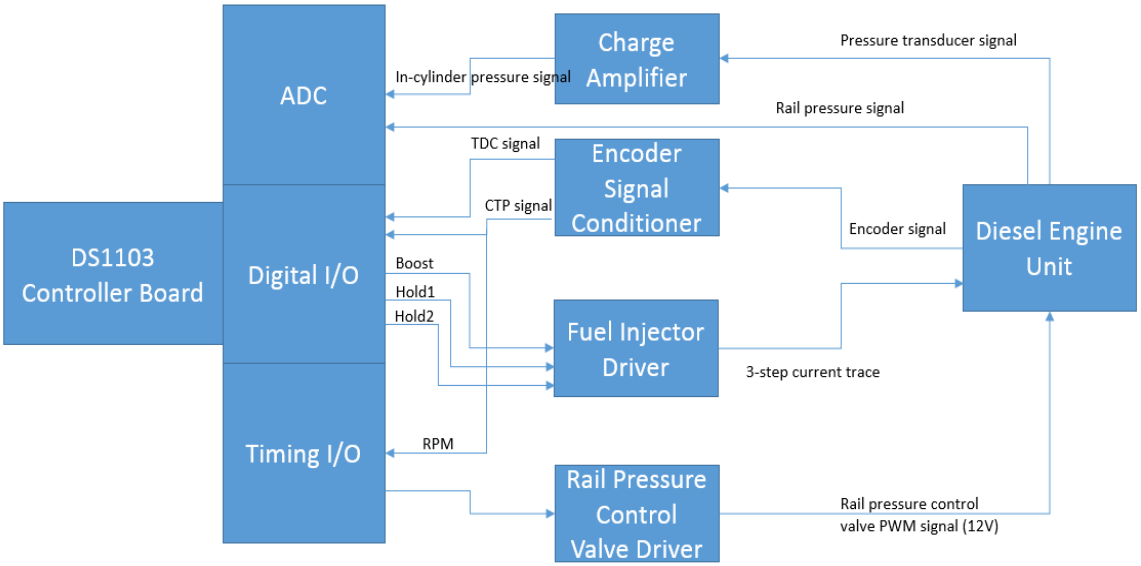

Figure 3.3. Schematic of Control System Signal Flow (Reproduced from [1]).

The electronic control unit used in this project is dSPACE DS1103 control board. It not only works with rail pressure sensor and regulator valve, but also communicates with the encoder that measures crank angle, and the pressure transducer, which reads the cylinder pressure. An illustrative scheme is shown in Figure 3.3, demonstrating how signals flow in the whole system. All measurements and control signals are crank-angle-based but the time vector is also recorded by dSPACE [1].

3.2 Acoustic Measurement

Noise from engines needs to be accurately measured in order to indicate the power level of acoustical emission. Ideally, engines should be placed in a free-field environment where there are no obstacles or reflecting surfaces, which generate stationary acoustic waves, and measurements should be taken over the whole surface of a virtual enclosure. However such a perfect free-field environment is not always practical and it is acceptable in engineering to take measurements in an essentially free-field over a reflecting surface, according to ISO 3744.

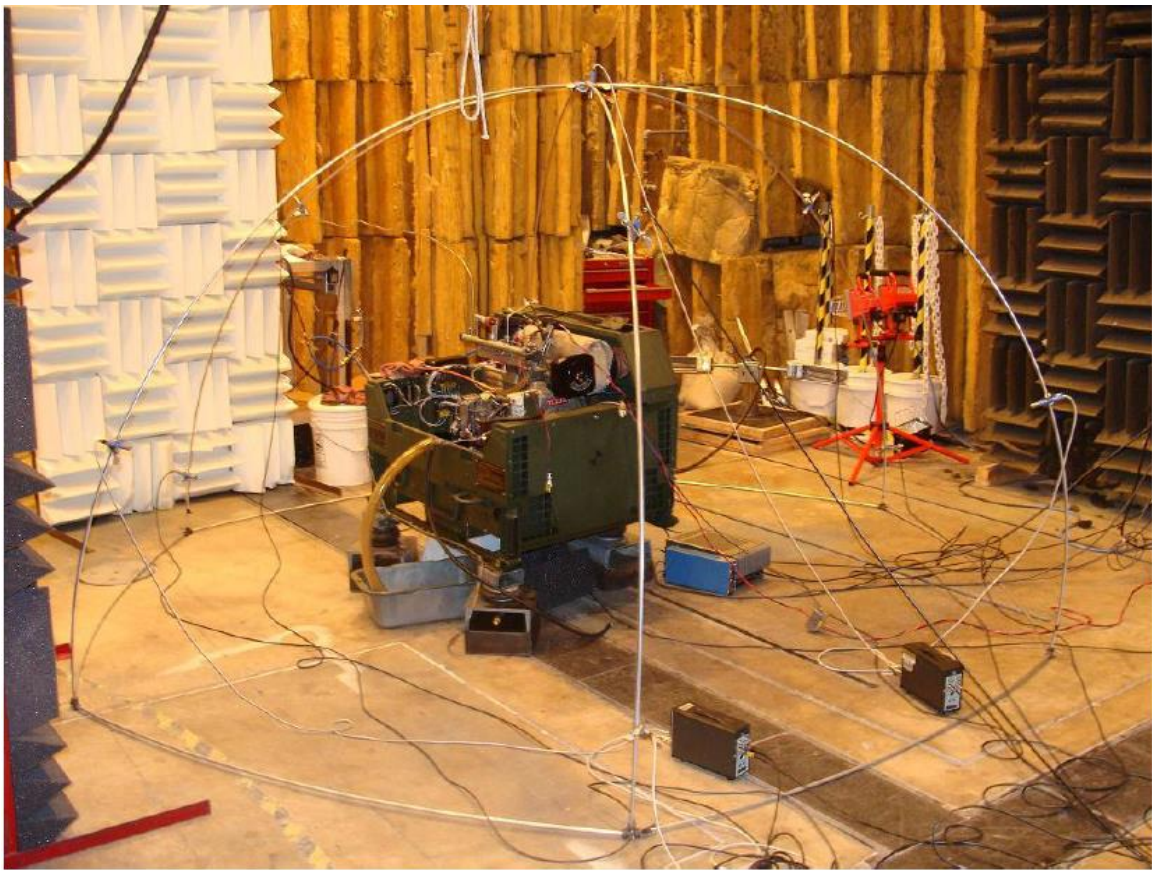

Figure 3.4. Sound pressure measurement setup in hemi-anechoic chamber [2].

Acoustic measurements generally start with a microphone that precisely measures the pressure variations around ambient atmospheric pressure and returns the quantity as a voltage. Power supplies and signal conditioners are often needed to supply current, polarize transducers, amplify charges and filter signal noise. In practice, a hemi-enclosure, rectangular or spherical, is used as surface for measurement. Figure 3.4 shows the acoustic measurement setup for this project. The engine was placed in a hemi-anechoic chamber where walls are coated with high sound-absorption foams but an acoustic reflecting floor plane is allowed. Such setup complies with the essential free-field environment described in ISO 3744 and is appropriate for acoustic measurement.

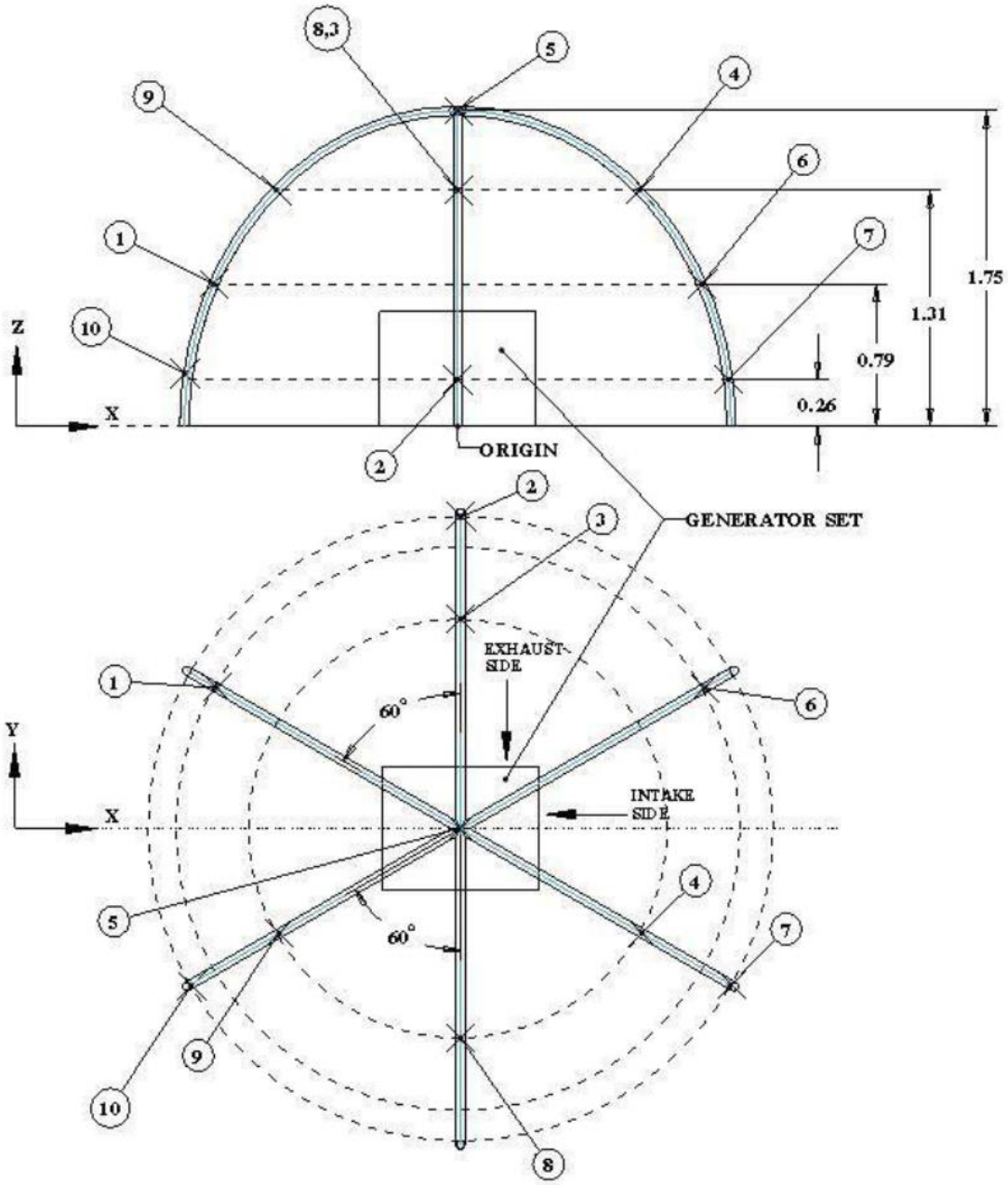

Figure 3.5. Locations of Microphones for Sound Pressure Measurement [2].

The hemisphere enclosure used is 1.75 m in radius and there are 10 microphones placed at different locations. The illustration and coordinates of microphone locations are shown in Figure 3.5 and Table 3.1.

Table 3.1. Coordinates of Microphone Locations for Sound Pressure Measurement (Reproduced from [2]).

Microphone Locations	x (m)	y (m)	z (m)
1	-1.35	0.78	0.79
2	0.00	1.73	0.26
3	0.00	1.16	1.31
4	1.00	-0.58	1.31
5	0.00	0.00	1.75
6	1.35	0.78	0.79
7	1.50	-0.87	0.26
8	0.00	-1.16	1.31
9	-1.00	-0.58	1.31
10	-1.50	-0.87	0.26

Since the range of sound pressure measurements varies greatly, a logarithm scale is commonly used and defines the sound pressure level:

$$SPL = 10\log(\frac{{p_{rms}}^2}{{p_{ref}}^2})\ \mathrm{dB} \tag{3.1}$$

where p_{rms} is the effective mean pressure and p_{ref} is the reference pressure, usually taken as the threshold of human hearing capability, 20 μPa.

An important rating in acoustics is the sound power. As opposed to sound pressure, which depends on the distance to the source and the properties of the media in which the sound travels, sound power is independent of the surroundings and is an indicator of the total energy emitting from a sound source. The sound power is defined as:

$$W = \int I \mathrm{d}S \tag{3.2}$$

where S is the surface area and I is the acoustic intensity defined as:

$$I = \frac{{p_{rms}}^2}{\rho_0 c} \tag{3.3}$$

where ρ_0 is the density of air, usually taken as $1.21\ \mathrm{kg/cm^3}$,

and c is the speed of sound in air, usually taken as $343\ \mathrm{m/s}$.

Sound power is also commonly represented in logarithm scale, and the sound power level is defined as:

$$SWL = 10\log(\frac{W}{W_{ref}})\ \mathrm{dB} \tag{3.4}$$

where W_{ref} is the reference sound power, expressed as:

$$W_{ref} = \frac{{p_{ref}}^2}{\rho_0 c} S_{ref} \tag{3.5}$$

where S_{ref} is taken as $1\ \mathrm{m}^2$, W_{ref} is around 10^{-12} W.

If the average sound pressure from 10 microphones is used to calculate the sound power in Equation (3.2), the relationship between sound power level and sound pressure level can be found as:

$$SWL = SPL + 10\log(\frac{S}{S_{ref}})\ \mathrm{dB} \tag{3.6}$$

The dB scale treats all frequencies equally, which does not reflect the nature of human hearing. Human ears are particularly sensitive to frequencies in a range from 1000 to 4000 Hz. The A-weighting filter approximates the hearing characteristics and was adopted by OSHA in 1972 as the official sound pressure level correction method [6].

In ANSI standards [18], the expression for A-weighting filter is:

$$W_A(f) = 10\log\left[\frac{1.562f^4}{(f^2+107.65^2)(f^2+737.86^2)}\right] + W_C(f)\ \mathrm{dB} \tag{3.7}$$

where

$$W_C(f) = 10\log\left[\frac{2.242\times10^{16}\cdot f^4}{(f^2+20.598^2)^2(f^2+12194.22^2)^2}\right]\ \mathrm{dB} \tag{3.8}$$

The A-weighted sound pressure level and sound power level are represented as:

$$SPL_A(f) = SPL(f) + W_A(f)\ \mathrm{dB(A)} \tag{3.9}$$

$$SWL_A(f) = SWL(f) + W_A(f)\ \mathrm{dB(A)} \tag{3.10}$$

where $\mathrm{dB(A)}$ indicates a frequency-A-weighting scale.

CHAPTER 4. ENGINE BLOCK STRUCTURAL ATTENUATION MODEL

In an attempt to understand and predict the noise radiated from engines, the structural attenuation, which captures all acoustic characteristics of the engine block, was studied in this thesis. This concept was first proposed by Austen and Priede [13] and then adopted by many researchers and even engine manufacturers as an indicator of engine performance in terms of acoustic emission. The attenuation model, however, was completely based on a linear assumption and any discrepancies during modeling were attributed to the non-negligible mechanically-induced noise, which was not supposed to be included in the linear part of the cylinder pressure – noise level relationship.

The focus of this thesis is to challenge the linear assumption of the engine block attenuation model and to investigate the impact of different nonlinearities on the behavior of the model. Measurements of cylinder pressure and corresponding noise level under several operating conditions were performed at the previous stage of the project and an attenuation model, represented as attenuation curve over a range of frequencies, was generated via a conventional linear approach. However, attenuation curves generated under different operating conditions were not consistent and therefore calls for study of the attenuation model from another perspective, in a nonlinear way.

Just as most nonlinear problems start with a linear approximation, a linear attenuation model that best describes the averaged characteristics of attenuation curves generated in different cases was set up. The model was represented in terms of an attenuation curve, transfer function, differential equations and finally a mass-spring-damper system. The physical system resembles the main characteristics of the original attenuation model, and provides freedom to easily build in nonlinearities such as nonlinear springs or dampers. Finally, through simulation of the mass-spring-damper model, the impact of nonlinearities was studied and compared with a purely linear model.

4.1 Assumptions of Engine Block Attenuation

The structural attenuation model of engine blocks comes with several important underlying assumptions. These assumptions lead to a straightforward definition of attenuation (Equation (2.1)) but also introduce inaccuracies in modeling the acoustic features of the engine block and subsequently account for some discrepancies when experimentally measuring and computing the attenuation. The major assumptions include:

1) Dominance of combustion-induced noise: The noise radiated from the engine is considered to be mainly, if not wholly, a result of forces excited by combustion. This includes both combustion forces that come directly from the variation of cylinder pressure and mechanical forces that come from the movement of various parts in the engine including piston, gear trains, crankshaft, etc. but only as a result of combustion. Mechanical forces that are independent of the combustion process are generally considered to have little contribution to the overall noise emission and thus are often neglected. Techniques to separate noise induced purely by mechanical forces independent of combustion, such as periodic piston movement or injector valves opening, are sometimes adopted but in most cases overlooked if there is no indication this could be a problem.
2) Cylinder pressure representative of combustion process: This assumption states that cylinder pressure alone is enough for fully describing the combustion process, at least from an acoustic perspective, and can be used solely to compare with the corresponding noise emission and compute the attenuation. While combustion does result in substantial variations in cylinder pressure, change of cylinder pressure cannot always be attributed to combustion. Cyclic piston movement, intake of air and emission of exhaust all contribute to cylinder pressure variations and don't necessarily have connections with a particular combustion process. Variations in cylinder pressure from these sources, however, excite noise from the engine block and consequently the difference of total cylinder pressure and noise radiation level still serves as a valid acoustical structural attenuation model for the engine block. Cylinder pressure decomposition can be realized by subtraction of cylinder pressure when the combustion is not present, usually the free rotating cycles when there is no fuel injection, from the measurements of cycles when fuel injection and subsequent combustion are present. Similar decomposition could also be applied to acoustic measurements of noise and the attenuation model generated would be between only combustion-related pressure variations and combustion-induced noise.
3) Linear assumption of engine block attenuation: The engine block attenuation can be regarded as a system that captures the acoustic characteristics of the engine block and takes cylinder pressure as input and noise radiation level as output. Figure 4.1 shows a schematic of the engine block attenuation system, which essentially attenuates the cylinder pressure inputs and results in sound pressure outputs at a certain distance from the center of the engine block, indicating the level of noise radiation. A linear attenuation model assumes the relationship between cylinder pressure and engine noise radiation to be purely linear. Just as any linear system, such model follows the rule of superposition and preserves frequency of harmonic input. In the frequency domain, the linear assumption indicates that only one attenuation curve independent of input, which reflects different operating conditions of the engine, is allowed since the net attenuation of different harmonic components should only be a function of frequencies. Computation of the difference of spectrum of cylinder pressure and noise radiation level is a purely linear approach and any discrepancies from different computations could possibly result from an invalid linear assumption, in addition to measurement uncertainties and computation errors.

This thesis mainly investigates the validity of the linear assumption but still carries out the remaining analysis based on the first two assumptions. Although the linear assumption is challenged, the linear approach of generating attenuation was still adopted throughout the study with the exception that, this time, discrepancies of attenuation curves from different computations were explained by the introduction of nonlinearities.

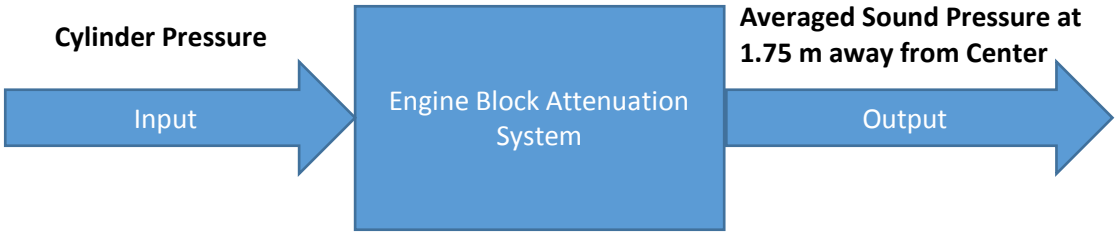

Figure 4.1. Schematic of Engine Block Attenuation System.

4.2 Attenuation Results from Experimental Measurements

To understand the impact of the combustion process on noise radiation, different injection strategies were tested during the previous phase of the project, among which the most studied was the injection timing of single injection pulses [2]. The injection into a diesel engine happens slightly before the piston hits top dead center (TDC) during the compression stroke of each cycle and the advancing time is measured in crank angles. The injection timing determines the start of combustion and subsequently the cylinder pressure shape and completeness of combustion, which directly relate to efficiency, emission and noise radiation of an engine. Generally speaking, an early injection would result in an early start of combustion, rapid rise in cylinder pressure and temperature, and consequently lead to higher efficiency, decreased emission of soot, but increased NO_x exhaust and noise levels.

Test runs of five different injection timings each under two different operating conditions in terms of engine speed and load were conducted. The injection timings vary between 12° before top dead center (BTDC) and 24° BTDC, while the operating conditions are idle speed at 3050 rpm and zero load, and full load with 3450 rpm.

For each of the 10 cases, both cylinder pressure and sound pressure were measured at the same time in the hemi-anechoic chamber (Figure 3.4). The cylinder pressure was measured by a pressure transducer preinstalled and the sound pressure was measured by 10 microphones at 1.75 m from the center of the engine (Figure 3.5). Attenuation was computed according to Equation (2.1) for each case and the detailed steps include:

1) Generate the 1/3 octave band spectrum of cylinder pressure level over frequencies from 20 to 20,000 Hz from time history of cylinder pressure measurements.
2) Generate the 1/3 octave band spectrum of sound pressure level over frequencies from 20 to 20,000 Hz from the averaged time history of 10 microphone measurements and apply A-weighting filter to the spectrum.

3) Compute the difference between 1/3 octave band spectra of cylinder pressure and of A-weighted sound pressure level and express the result as an attenuation curve over frequencies from 20 to 20,000 Hz.

The resulting attenuation curves of different injection timings under different operating conditions are plotted in Figures 4.2 and 4.3.

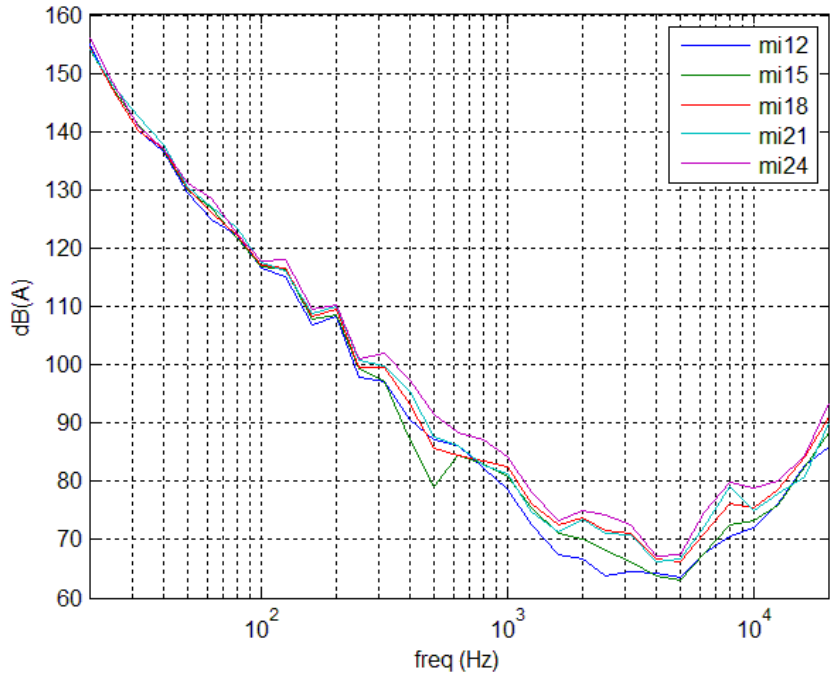

Figure 4.2. Attenuation Curves for the Engine Block with Various Injection Timings for Single Injection at Idle Speed [2].

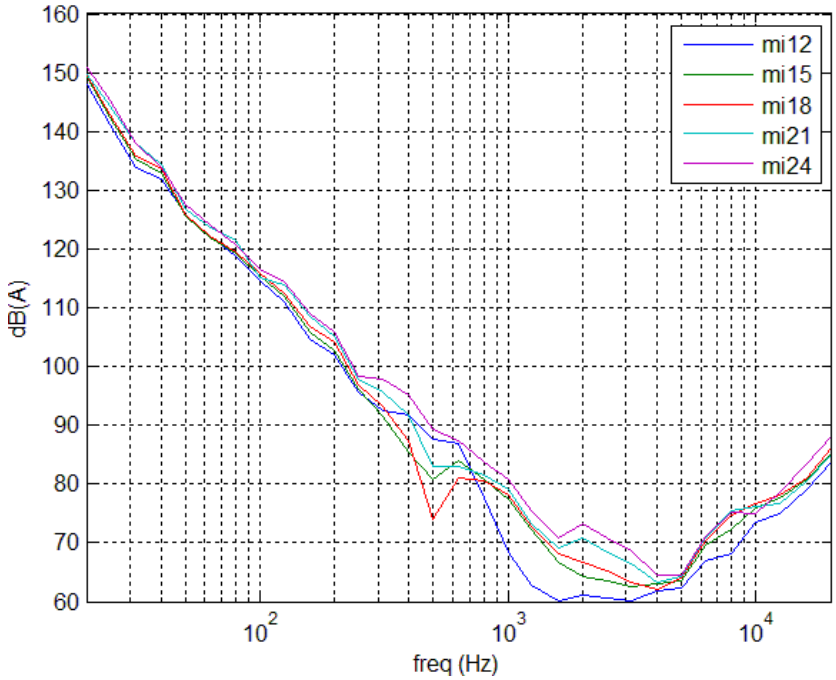

Figure 4.3. Attenuation Curves for Engine Block with Various Injection Timings for Single Injection at Full Load [2].

Significant discrepancies can be observed from these attenuation curves with different injection timings for each operating condition although general trends are similar. Attenuation is relatively low over high frequencies and is least around 5,000 Hz. Lower attenuation means greater contribution of cylinder pressure to the overall noise level and thus it is important to understand the discrepancies in the range of high frequencies where the attenuation is low, by introduction of a new model.

Note that although it is more important to focus on the range of high frequencies, the discrepancies among different attenuation curves don't necessarily grow with frequencies. Since the attenuation is represented in a logarithm scale, a fixed difference in dB indicates a fixed percentage variation and the absolute differences grow as the base level increases. Hence the discrepancies in low frequency range could be as significant as in high frequency range because the averaged attenuation is much higher in low frequency range than in high frequency range, although in a logarithm scale discrepancies in high frequency range seem dominant.

There is a noticeable amplitude shift of attenuation curves for different injection timings in both idle and full load cases, and the shift appears to be in sequence of the advanced timing of injection. Namely, the attenuation of the earliest injection is the highest whilst a late injection accompanies a low attenuation. Since early injection also increases both the peak of cylinder pressure itself and the rise rate, the change of attenuation can be accounted for by change of amplitude of the input to the system, which is cylinder pressure. Qualitatively, larger amplitude of cylinder pressure input results in a higher attenuation. This behavior is very similar to that of a typical nonlinear system and hence a nonlinear model was built to verify the hypothesis.

There are also other discrepancies among the attenuation curves, although less evident or seemingly of little causality with the injection timings or operating conditions. For instance, a sub-resonant peak around 500 Hz is found only in some cases of different injection timings. To judge whether these behaviors are also the results of nonlinearities in the attenuation model requires the construction of a nonlinear model first.

4.3 Modeling and Simulation

Representing the acoustic characteristics of an engine block with an attenuation curve, generated from differences of input cylinder pressure spectrum and output sound pressure level spectrum, is a purely linear approach. In order to incorporate nonlinearities, the attenuation curves need to be transformed into another representation that applies to both linear and nonlinear systems. The most fundamental mathematical representation of a system would be differential equations. The modeling procedure in this thesis started with an averaged linear attenuation curve, estimated the transfer function and converted it into differential equations and an equivalent mass-spring-damper model. A virtual mass-spring-damper model was then developed and simulated with the help of MATLAB SIMULINK.

4.3.1 Averaged Magnitude-Frequency Response and Estimated Transfer Function

The modeling started with a linear approximation that essentially takes the average of the attenuation curves corresponding to various injection timings. The operating condition used for modeling is idle speed and the full load condition is reserved for model validation purpose.

The attenuation curve is essentially a mirror image of the conventional magnitude-frequency response curve of a system with respect to the 0 dB axis, and a transfer function can be readily estimated to match the general trends of the curve. Approximately speaking, the averaged attenuation decreases at a rate of 40 dB/decade until reaching its minimum around 5,000 Hz and increases afterwards at the same rate. This resembles a 4^{th} order system with 2 zeros. The system can be decomposed into 2 second-order systems each representing the magnitude-frequency response of cylinder pressure and averaged sound pressure, and the A-weighting filter, respectively. Since A-weighting filter is well-defined and can be readily imposed during spectrum analysis, it is temporarily taken out to lower the degree and complexity of the engine block attenuation system.

The simplified engine block attenuation system (Figure 4.1) takes cylinder pressure as input and averaged noise pressure measured at a set distance (1.75 m) from the center of the engine as output. The resulting averaged magnitude response when the engine is at idle is plotted in Figure 4.4 as the blue curve. Compared to the attenuation curves in Figure 4.2, the magnitude response curve changes at a rate of $\pm 20\ \mathrm{dB/decade}$ instead of $\pm 40\ \mathrm{dB/decade}$, and there is a break frequency around 100 Hz in addition to the resonant frequency around 5,000 Hz. The differences can be accounted for by taking out the A-weighting filter, which is essentially a 2^{nd} order system.

The estimated transfer function is of 2nd order with 1 zero and the expression is:

$$\frac{Y(s)}{U(s)} = \frac{k_a(s+\omega_b)}{s^2+2\zeta\omega_n s+{\omega_n}^2} \tag{4.1}$$

where $U(s)$ is the Laplace transform of $u(t)$, cylinder pressure and input to the attenuation system

$Y(s)$ is the Laplace transform of $y(t)$, averaged sound pressure and output of the system

gain $k_a = 11.885$

break frequency $\omega_b = 2\pi \times 100 = 628.319 \text{ rad/s}$

damping ratio $\zeta = 0.35$

natural frequency $\omega_n = 2\pi \times 5{,}000 = 31{,}415.927 \text{ rad/s}$

The magnitude response of the estimated transfer function is plotted in green against the averaged experimental response in Figure 4.4. The estimated transfer function, matching only general trends of the experimental response, does not contain information of all the details, but provides a model that is simple enough to implement and explore nonlinearities.

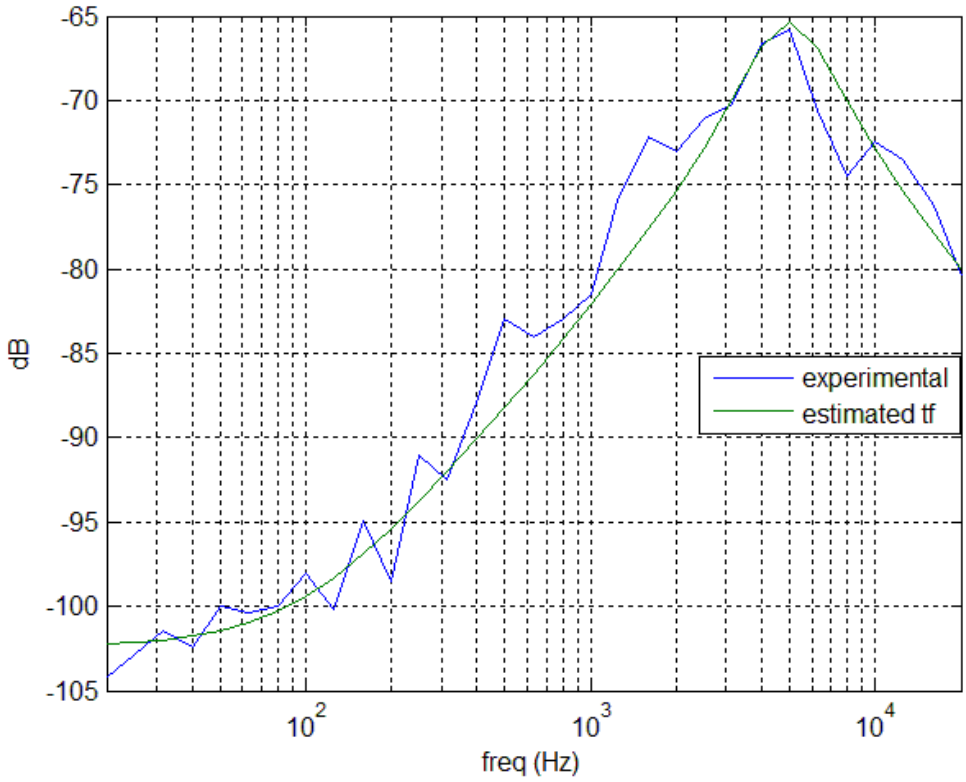

Figure 4.4. Magnitude-Frequency Responses of the Engine Block Attenuation System at Idle Speed (Blue: Averaged Experimental Attenuation Curves; Green: Simulated Attenuation Curves from Transfer Function in Equation (4.1)).

4.3.2 Spring-Mass-Damper Model

A transfer function still remains a representation of only linear systems. In order to introduce nonlinearities, it needs to be converted to differential equations or an equivalent physical model. Due to the nature of the transfer function obtained in Equation (4.1), a simple mass-spring-damper system is able to represent the 2nd order system with a zero.

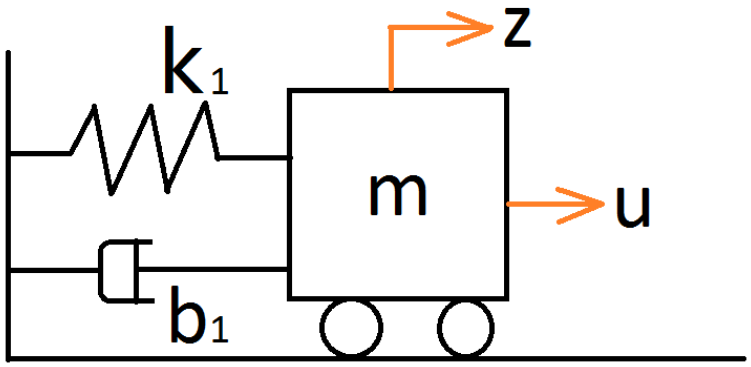

Figure 4.5. Schematic of a Spring-Mass-Damper System.

Figure 4.5 illustrates a typical mass-spring-damper system where m, k_1, b_1 are mass, linear spring constant and linear damper constant, respectively, and u is the external force exerted on the mass block and z is the displacement of the mass. The equation of motion of the system can be written as:

$$m\ddot{z} + b_1\dot{z} + k_1 z = u \tag{4.2}$$

Taking Laplace transformation of both sides and rearranging, we get:

$$\frac{Z(s)}{U(s)} = \frac{1}{ms^2+b_1 s+k_1} \tag{4.3}$$

To construct a 2nd order system with a zero, let $x = \dot{z}$ and Equation (4.2) can be rewritten as:

$$m\dot{x} + b_1 x + k_1 \int x = u \tag{4.4}$$

Taking Laplace transformation results in:

$$\left(ms + b_1 + \frac{k_1}{s}\right) X(s) = U(s) \tag{4.5}$$

Rearranging, we have:

$$\frac{X(s)}{U(s)} = \frac{s}{ms^2+b_1 s+k_1} \tag{4.6}$$

The output of the system can be chosen as a linear combination of displacement z and velocity x, which can be expressed as:

$$\begin{aligned}\frac{Y(s)}{U(s)} &= C_0\frac{Z(s)}{U(s)} + C_1\frac{X(s)}{U(s)} \\ &= \frac{C_1 s + C_0}{ms^2 + b_1 s + k_1} \\ &= \frac{\frac{C_1}{m}(s + \frac{C_0}{C_1})}{s^2 + \frac{b_1}{m}s + \frac{k_1}{m}}\end{aligned} \tag{4.7}$$

Equating Equations (4.1) and (4.7), the parameters of the mass-spring-damper system can be determined:

$$\begin{cases} k_a = \frac{C_1}{m} \\ \omega_b = \frac{C_0}{C_1} \\ 2\zeta\omega_n = \frac{b_1}{m} \\ {\omega_n}^2 = \frac{k_1}{m} \end{cases} \tag{4.8}$$

Taking $m = 1\ \text{kg}$, the remaining parameters can be calculated:

$$\begin{cases} k_1 = m{\omega_n}^2 = 9.87 \times 10^8\ \text{N/m} \\ b_1 = m(2\zeta\omega_n) = 2.20 \times 10^4\ \text{N} \cdot \text{s/m} \\ C_1 = mk_a = 11.885 \\ C_0 = C_1\omega_b = 7467.57 \end{cases} \tag{4.9}$$

The system can also be written in state-space form where the state variables are $x_1 = z$ and $x_2 = \dot{z}$:

$$\begin{aligned} &\begin{bmatrix}\dot{x}_1 \\ \dot{x}_2\end{bmatrix} = \begin{bmatrix}0 & 1 \\ -\frac{k_1}{m} & -\frac{b_1}{m}\end{bmatrix}\begin{bmatrix}x_1 \\ x_2\end{bmatrix} + \begin{bmatrix}0 \\ \frac{1}{m}\end{bmatrix}u = \begin{bmatrix}x_2 \\ -\frac{k_1}{m}x_1 - \frac{b_1}{m}x_2 + \frac{1}{m}u\end{bmatrix} \\ &y = \begin{bmatrix}C_0 & C_1\end{bmatrix}\begin{bmatrix}x_1 \\ x_2\end{bmatrix} \end{aligned} \tag{4.10}$$

With the introduction of a nonlinear spring and damper, a nonlinear model can be readily constructed. For simplicity, only one cubic nonlinear term is added.

Spring force is expressed as:

$$F_s = k_1 z + k_3 z^3 \tag{4.11}$$

Damper force is expressed as:

$$F_d = b_1\dot{z} + b_3\dot{z}^3 \tag{4.12}$$

The reason to choose a cubic term other than a quadratic term is that the cubic term preserves the oddness of the original expression of spring force and damper force and ensures that the direction of force always aligns with the direction of displacement or velocity.

Implemented with a nonlinear spring and damper, the differential equations in Equation (4.10) can be rewritten as:

$$\begin{bmatrix}\dot{x}_1\\ \dot{x}_2\end{bmatrix}=\begin{bmatrix}x_2\\ -\frac{k_1}{m}x_1-\frac{k_3}{m}{x_1}^3-\frac{b_1}{m}x_2-\frac{b_3}{m}{x_2}^3+\frac{1}{m}u\end{bmatrix}$$
$$y=\begin{bmatrix}C_0 & C_1\end{bmatrix}\begin{bmatrix}x_1\\ x_2\end{bmatrix} \quad (4.13)$$

4.4 Model Parameter Estimation

In order to facilitate implementation of nonlinearities, a SIMULINK model was built for simulation as shown in Figure 4.6. Simscape toolbox was used to build the physical system of mass, spring and damper. Nonlinear translational spring and damper elements are integrated in the system and both linear and nonlinear coefficients k_1, k_3, b_1 and b_3 are variables controllable in the workspace. Such configurations provide maximum flexibility for parametric tuning as adding a nonlinear term would generally call for a decrease in the linear term to compensate for the effect.

The input to the simulated physical mass-spring-damper system comes directly from the experimental measurements of cylinder pressure. The main purpose of the model is to be able to predict corresponding noise radiation given only the cylinder pressure measurements, serving similarly as the attenuation curve based on a linear model assumption. The ability and validity of sound power prediction would be discussed in the next chapter and this chapter mainly focuses on the attenuation curves generated from models with different nonlinearities and compares them with the ones generated entirely by the experimental measurements.

The detailed procedures for computing simulated attenuation curves are:

1) Feed in experimental measurements of cylinder pressure, re-sampled evenly at 40,000 Hz as opposed to the crank-angle-based uneven sampling of the original measurements.
2) Run the SIMULINK model and export the simulated sound pressure measurements, also sampled evenly at 40,000 Hz.
3) Compute the 1/3 octave band spectra of re-sampled experimental cylinder pressure and the simulated sound pressure measurements with A-weighting.
4) Compute the difference between the two 1/3 octave band spectra and record it as an attenuation curve.

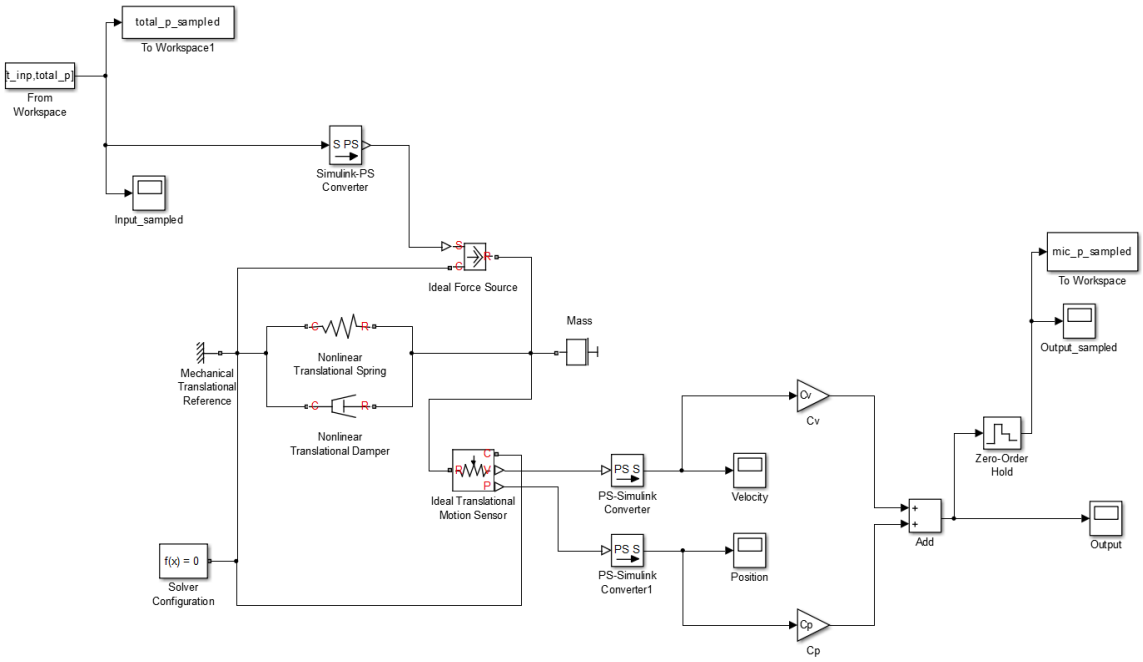

Figure 4.6. Simulink Block Diagrams of Mass-Spring-Damper Model.

Due to the inability to generate genuine experimental measurements, the experimental cylinder pressure used for simulation is not the exact one that was used to compute the attenuation curves in Figures 4.2 and 4.3. Instead, measurements taken at a different time, not identical but still representative of variations of pressure level corresponding to different injection timings, were used as inputs to the simulation model. Figure 4.7 shows the set of cumulative cylinder pressure level measurements at idle speed, and it can be observed that the cylinder pressure increases as injection is advanced with more crank angle degrees. Inaccuracies of predictions can be expected, since the experimental attenuation curves have demonstrated dependence on input, but they should not be significant, and would not affect the study and comparison of qualitative impact of different nonlinearities on behaviors of attenuation curves.

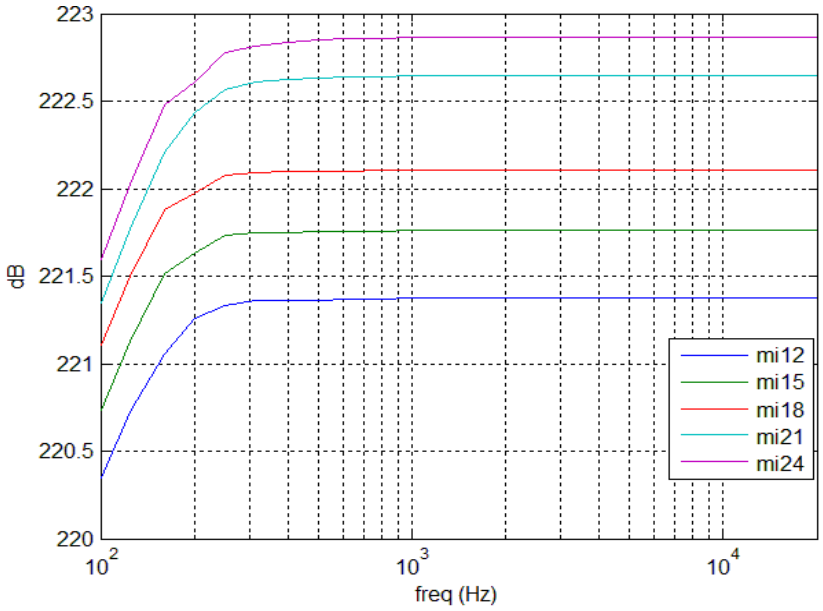

Figure 4.7. Experimental Cumulative Cylinder Pressure for Various Advanced Crank Angles of a Single Injection Pulse (Idle Speed).

The first case tested was a purely linear model, and as expected, the attenuation curves for a linear model where k_3 and b_3 equal zero overlap with each other (Figure 4.8). The resulting one attenuation curve, independent of injection timings, should exactly match the magnitude response of the estimated transfer function in Figure 4.4 except the response is flipped over and an A-weighting correction is added.

The degree of matching of the simulation model and the actual engine block attenuation system is quantitatively defined by the root mean square error between the simulated attenuation curves and the experimental attenuation curves. The errors are computed in dB over all frequency points on the 1/3 octave band spectra. Note that since the attenuation among low frequencies is higher, the same amount of difference in dB as among high frequencies actually indicates greater discrepancies in power density. By computing the unweighted root mean square error over the whole frequency range, effectively more weight is assigned to errors where attenuation is lowest. Since the region with the lowest attenuation also represents the major range of frequencies where noise is most prevalent, the root mean square error is a reasonable indicator of the quality of a model.

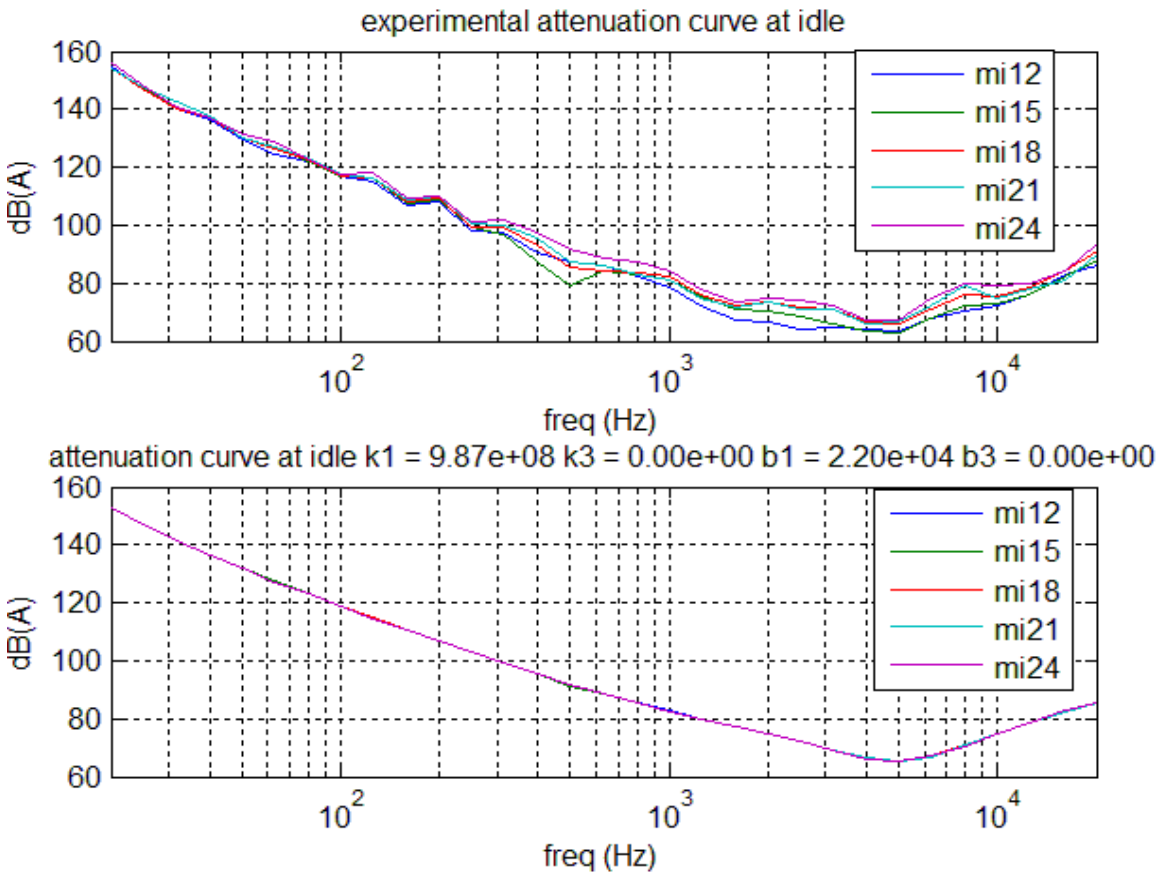

Figure 4.8. Comparison of Experimental Attenuation (top) and Simulated Attenuation (bottom) at Idle Speed (Linear Model).

Table 4.1. Root Mean Square Errors of Simulated Attenuation Curves with Different Model Parameters (Idle).

Test Cases	k_1 (N/m)	k_3 (N/m^3)	b_1 (N · s/m)	b_3 (N · s^3/m^3)	Averaged RMS Error (dB)
Linear	9.87×10^8	0	2.20×10^4	0	3.258
Nonlinear Damper Only	9.87×10^8	0	7.00×10^3	2.00×10^3	3.112
Nonlinear Spring and Damper (same damper as previous)	8.00×10^8	1.00×10^{13}	7.00×10^3	2.00×10^3	4.852
Nonlinear Spring and Damper (Optimized)	8.37×10^8	1.00×10^{13}	6.00×10^3	4.00×10^3	4.846

By changing coefficients of nonlinear spring and damper elements, models with different parameters are generated and simulated to compute the attenuation curve. A summary of some representative test cases is given in Table 4.1. In addition to the linear case, a nonlinear damper-only case and two nonlinear spring and damper cases were tested. The parameters in each case were tuned to minimize the root mean square error given any restrictions. For example, the nonlinear damper-only case keeps the spring elements the same as for the linear case but changes the linear and nonlinear coefficients of the nonlinear damper simultaneously to find the best combination. The test cases with both nonlinear spring and damper are divided into one with the same damper element as the nonlinear damper-only case, and one with both spring and damper coefficients tunable to get the best performance.

The nonlinear damper-only model slightly outperforms the linear model due to its better description of discrepancies among attenuation curves over high frequency ranges. From Figure 4.9, we can conclude that an inherent nonlinear damper is the reason for the amplitude shift of different attenuation curves. This can be explained by the higher effective damping as the input amplitude of cylinder pressure level goes higher, which takes place when more advanced injection timing is adopted, resulting in an increase of attenuation as the injection gets earlier.

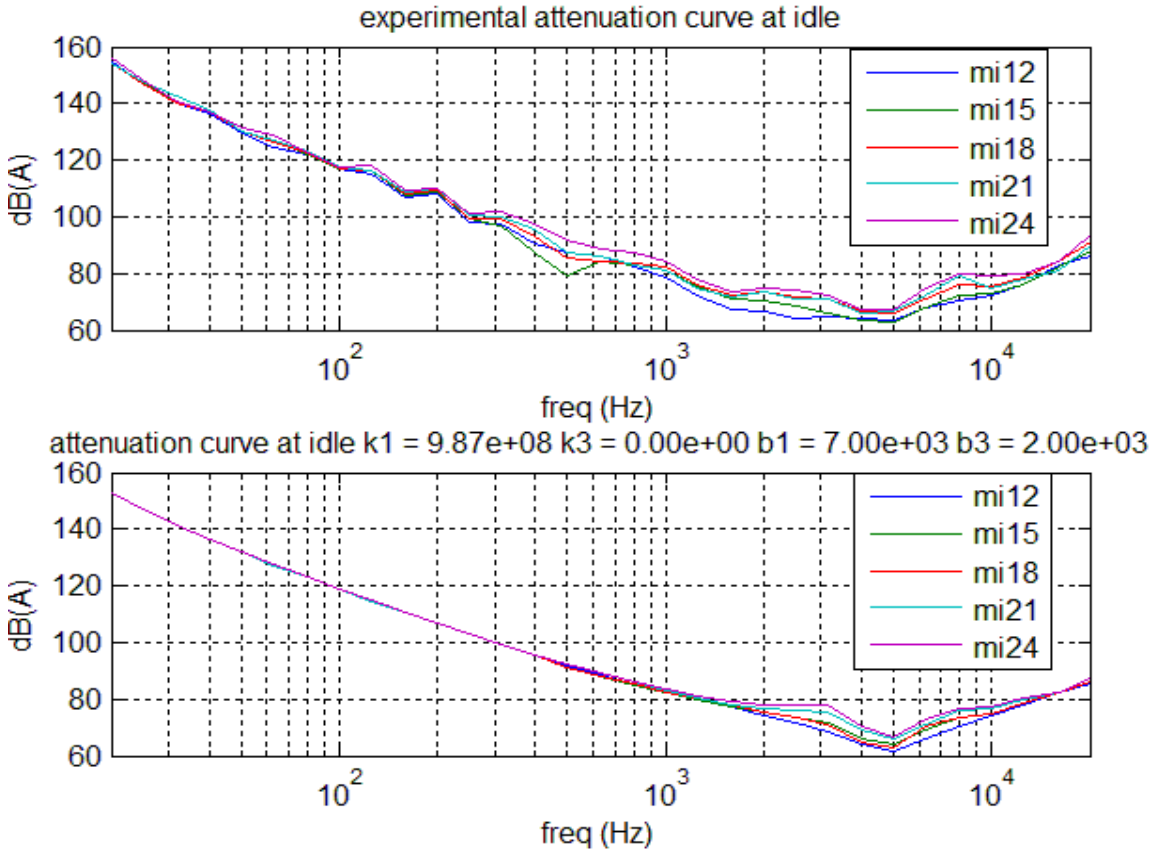

Figure 4.9. Comparison of Experimental Attenuation (top) and Simulated Attenuation (bottom) at Idle Speed (Nonlinear Damper-Only Model).

While including both nonlinear spring and damper elements increases the overall error, the discrepancies between different attenuation curves are very similar (Figure 4.10). In analogy to the amplitude-shift effect on resonant peaks brought by a nonlinear damper, theoretically a nonlinear spring should impose a shift in frequency for resonant peaks. However, such shift is not evident in the experimental attenuation curves and whether a nonlinear spring element is necessary in modeling needs to be analyzed through other observations, which, if any, match the experimental measurements. Fortunately, the first observation is that a nonlinear spring is responsible for expanding the bandwidth of resonant peaks. The flatter shape of the resonant region, compared to the shape generated from a model without nonlinear spring, agrees with the shape of the actual experimental attenuation curves. Another interesting observation is that with a nonlinear spring incorporated in the model, the MI15 and MI18 cases display similar sub-resonant peaks around 500 Hz. The cause of such sub-resonance is still unknown but the similarity between experimental attenuation and simulated attenuation indicates a potential relationship with the nonlinearities associated with spring elements.

Although the shapes of attenuation curves from a simulation model with nonlinearities included in both spring and damper elements do agree with the experimental results in many respects, the averaged root mean square error still gets larger compared to the linear case mainly because the nonlinear spring causes the attenuation curve to bend upwards between 300 Hz to 3,000 Hz. This could possibly be resolved by tuning a better combination of the four parameters, namely the linear and nonlinear coefficients of the spring and damper elements, of the nonlinear model or adding new kinds or more degrees of nonlinearities.

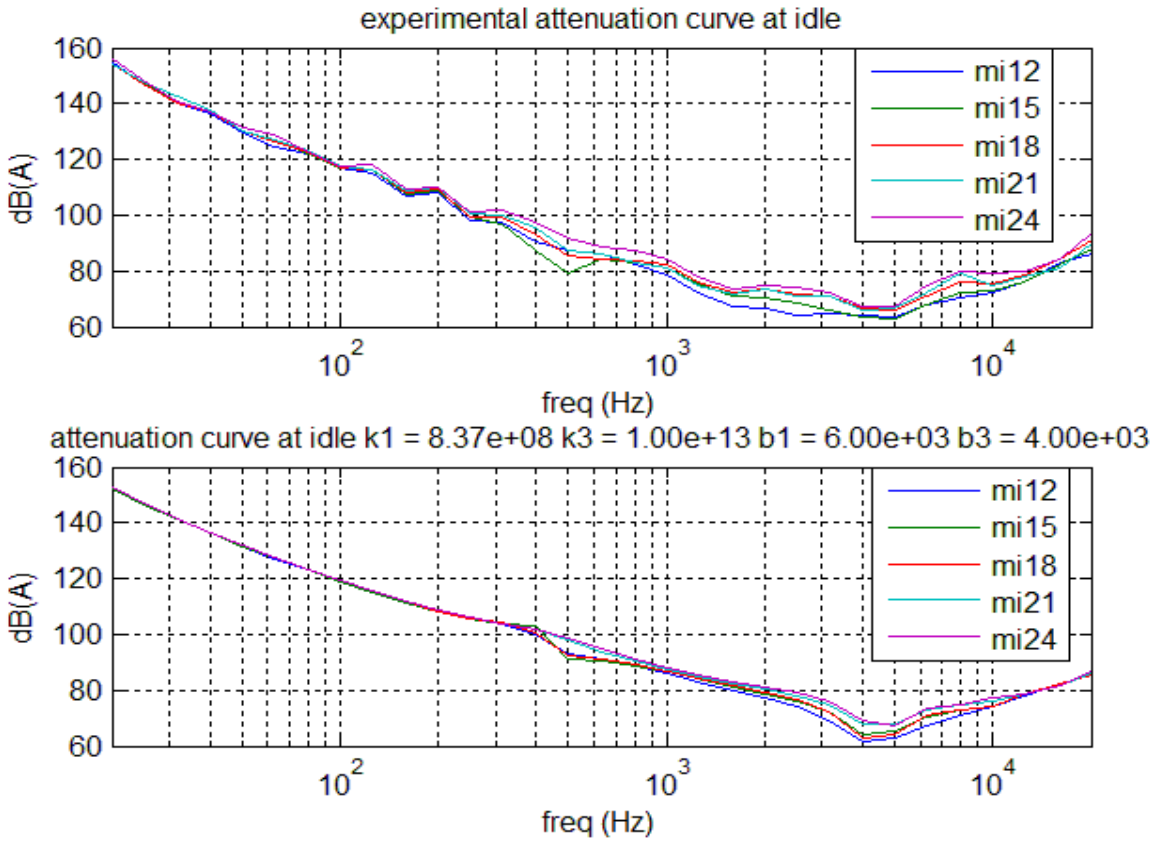

Figure 4.10. Comparison of Experimental Attenuation (top) and Simulated Attenuation (bottom) at Idle Speed (Optimized Nonlinear Spring and Damper Model).

To better illustrate the accuracies of attenuation models generated with different nonlinearities, the absolute errors between simulated and experimental attenuation curves were computed and averaged over 5 cases for different injection timings. The results, errors as a function of frequencies, are plotted in Figure 4.11. It can be observed that the purely linear model and the nonlinear damper-only model have the least errors and the nonlinear damper-only model shows improved accuracy in a range approximately from 5,000 Hz to 10,000 Hz, where the attenuation curves show resonance and have the least values. A nonlinear spring, however, tends to increase the errors even when the shapes of both experimental and simulated attenuation curves look more similar. When adding a nonlinear spring directly to the nonlinear damper-only model, the errors actually get larger, not only significantly between 300 Hz and 3,000 Hz, but also between 5,000 Hz and 10,000 Hz, where a nonlinear damper improved the accuracy already. Further tuning of the nonlinear damper does bring down the errors over high frequencies, but the significant errors between 300 Hz and 3,000 Hz prevail as a result of the inherent inaccuracies introduced by nonlinear spring elements.

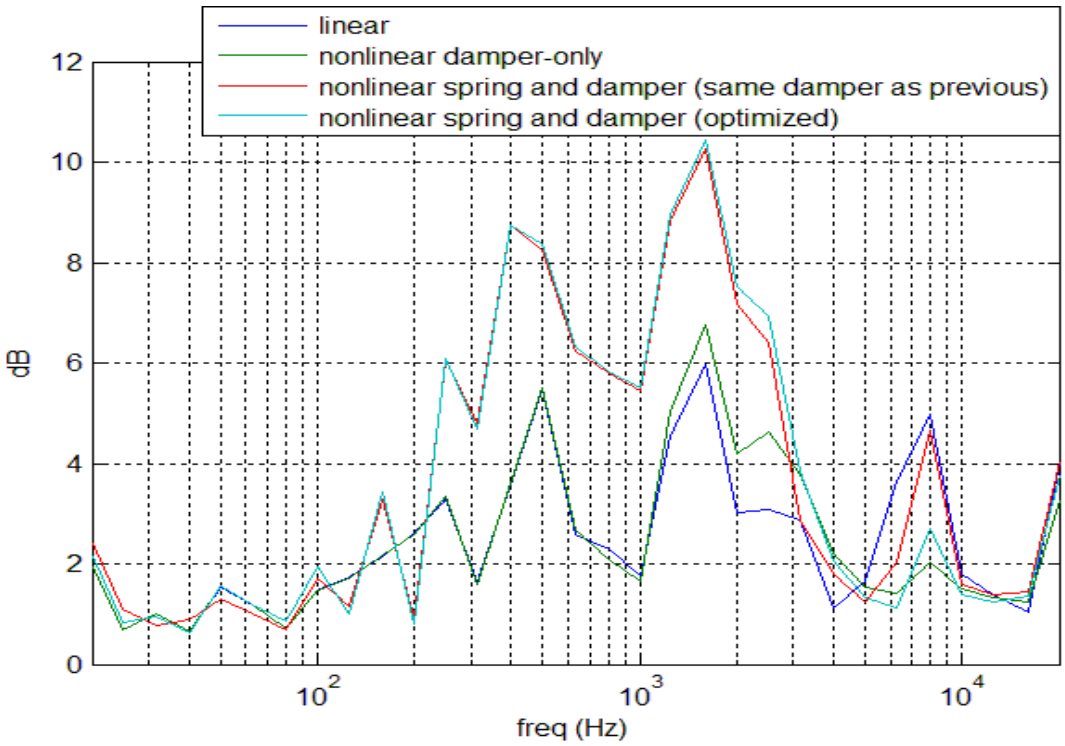

Figure 4.11. Absolute Averaged Errors between Simulated and Experimental Attenuation Curves (Idle Speed).

In conclusion, quantitatively a model with a linear spring and a nonlinear damper gives the most accurate description of the actual system, especially in frequency ranges above 5,000 Hz. Qualitatively, a model with both nonlinear spring and damper best agrees with the trends of discrepancies demonstrated in the experimental attenuation curves, but due to undesirable distortion of some portion of the curve in the mid-frequency range, the overall performance is not preferable.

4.5 Model Validation

All the attenuation models built so far were based on experimental data measurements taken when the engine was at idle speed. As the attenuation model represents the acoustic characteristics of the engine block itself and should be independent of the operating conditions, the model was validated with the experimental measurements taken when the engine was at full load.

Namely, first the virtual attenuation model or the mass-spring-damper system is adjusted, in terms of the four coefficients k_1, k_3, b_1 and b_3 for the nonlinear spring and damper elements, to reach the least error possible compared with the experimental attenuation curves measured when the engine is at idle speed. The simulation of the mass-spring-damper system at this point takes a set of cylinder pressure data that was also measured when the engine was at idle, not necessarily identical to measurements used to compute the experimental attenuation curves as

shown in Figure 4.2, but representative enough for typical cylinder pressure profiles at idle with various injection timings. The simulated output, which represents the sound pressure measured 1.75 m from the center of the engine block, is computed and compared with the cylinder pressure input in the frequency domain to get an attenuation curve.

Subsequently, the same virtual model is used to simulate inputs of a set of cylinder pressure data measured when the engine is at full load. Figure 4.12 shows a set of experimental measurements of cumulative cylinder pressure level when the engine is at full load. As for the idle case, the pressure level is generally higher for earlier injection except for the “mi21” and “mi24” cases where cumulative pressure levels are nearly identical. The resulting outputs from the model, which represent simulated sound pressure measurements, are compared with the input full-load cylinder pressure to give the simulated attenuation curves. This approach tests the ability of the virtual model to predict attenuation curves under different operating conditions, and thus justifies whether the model is robust enough.

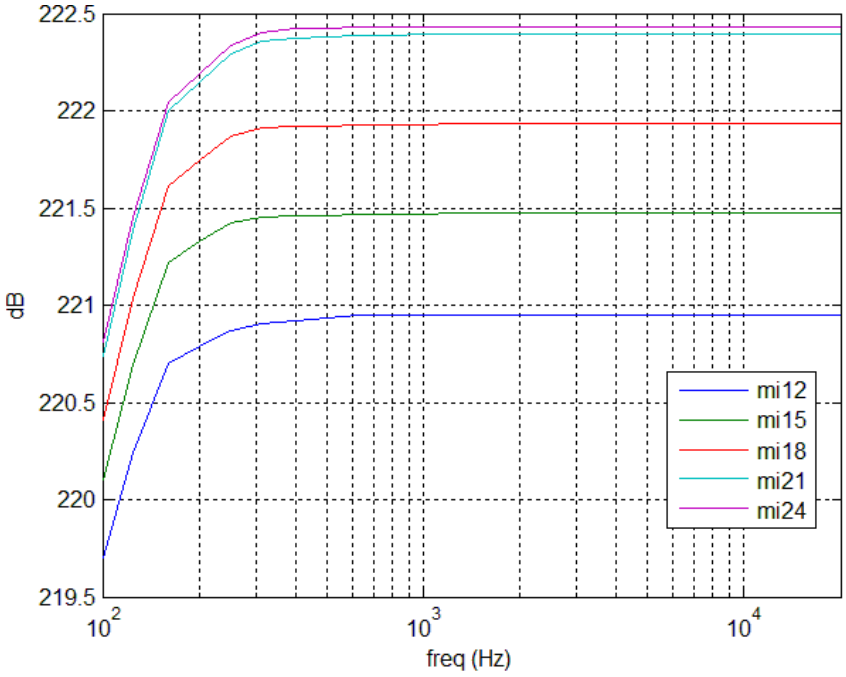

Figure 4.12. Experimental Cumulative Cylinder Pressure for Various Advanced Crank Angles of a Single Injection Pulse (Full Load).

Models built with linear spring and damper, linear spring but nonlinear damper and both nonlinear spring and damper, same as those used in the last section, were compared with the experimental measurements, in terms of attenuation curves and results are plotted in Figures 4.13, 4.14 and 4.15, respectively.

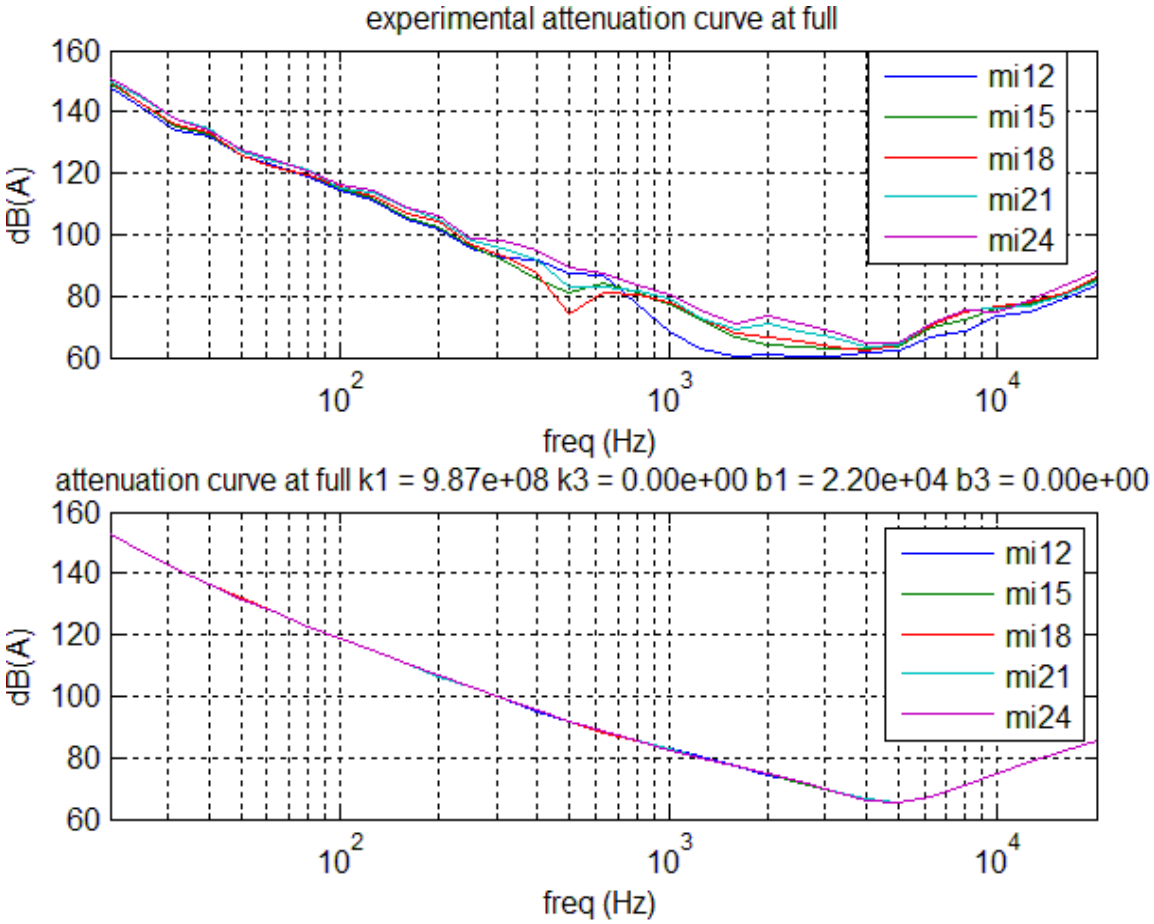

Figure 4.13. Comparison of Experimental Attenuation (top) and Simulated Attenuation (bottom) with Full Load (Linear Model).

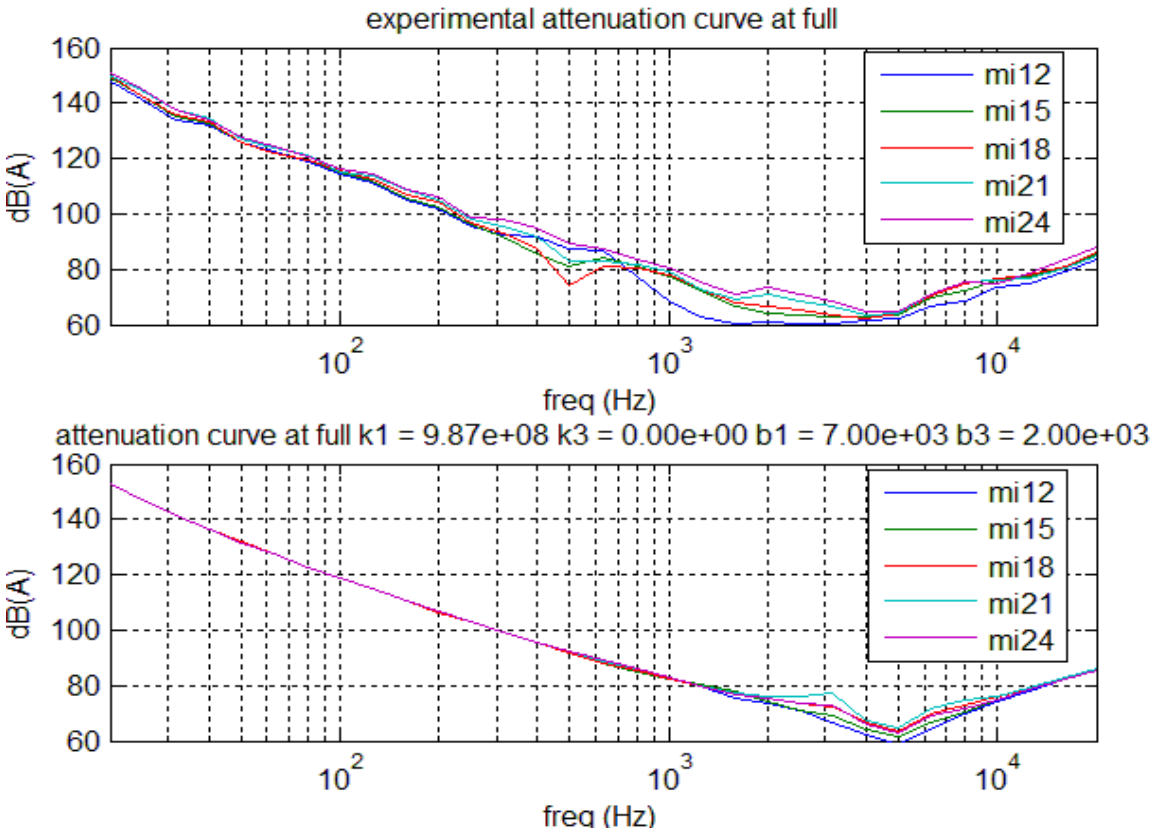

Figure 4.14. Comparison of Experimental Attenuation (top) and Simulated Attenuation (bottom) with Full Load (Nonlinear Damper-Only Model).

Figure 4.13 shows the attenuation curves calculated from simulation of a purely linear model. Not surprisingly, attenuation curves for different injection timings overlap perfectly and they are identical to what are calculated for the idle speed case (Figure 4.8). This linear result, as mentioned before, is essentially a combination of the A-weighting filter and the magnitude-frequency response of the mass-spring-damper model, which is an approximation of the actual response of the engine block attenuation over averaged measurements of attenuation curves for various injection timings at idle speed.

Figure 4.14, which shows the attenuation curves generated from the nonlinear damper-only model, similarly to simulation results for the idle case in Figure 4.9, features a separation of curves around the resonant frequency. The amplitude shift of the attenuation curves still follows the amplitude of input cylinder pressure in general, except the “mi21” case where the greatest attenuation is demonstrated. The exception could be explained by the actual cylinder pressure input at “mi21”. As shown in Figure 4.12, the cumulative cylinder pressure levels are close for both “mi21” and “mi24”, ranking the highest among all the cases. Hence, it is not surprising that the simulated attenuation curves would show the largest attenuation for the “mi21” case given this particular set of cylinder pressure inputs.

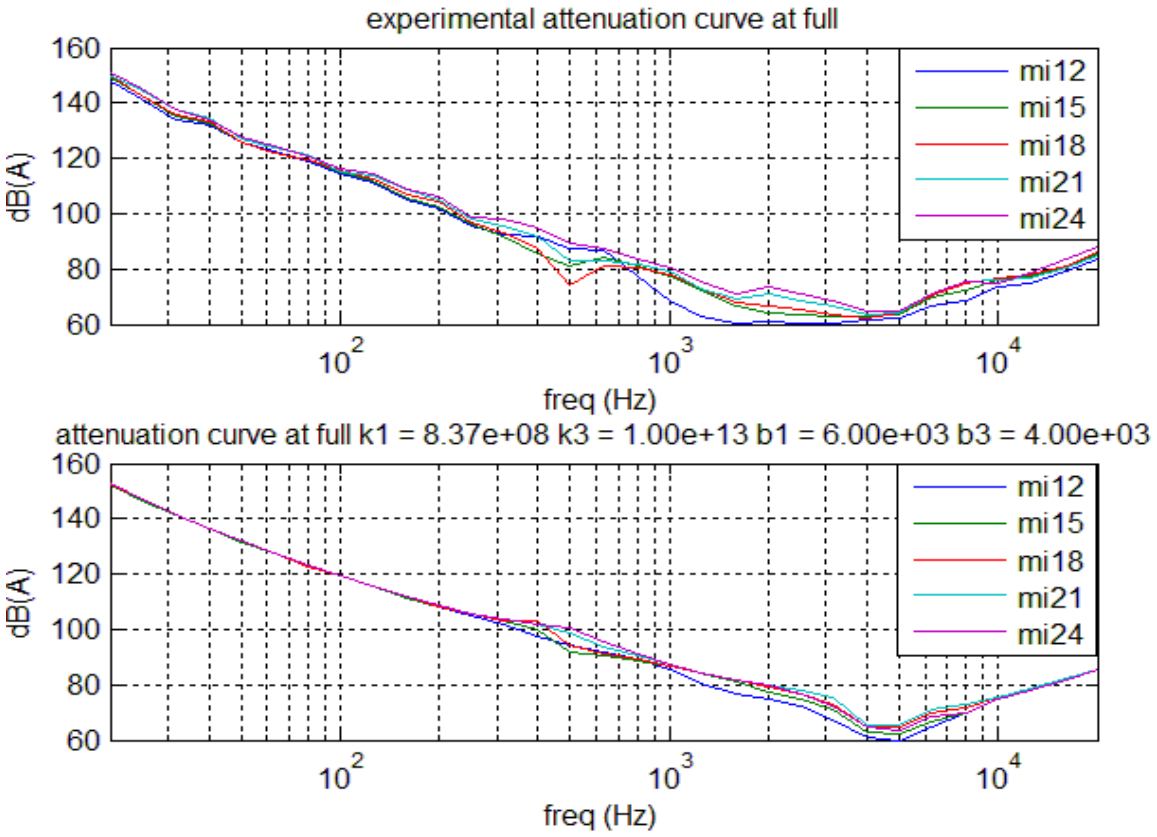

Figure 4.15. Comparison of Experimental Attenuation (top) and Simulated Attenuation (bottom) with Full Load (Optimized Nonlinear Spring and Damper Model).

Table 4.2. Root Mean Square Errors of Simulated Attenuation Curves with Different Model Parameters (Full Load).

Test Cases	k_1 (N/m)	k_3 (N/m^3)	b_1 (N · s/m)	b_3 (N · s^3/m^3)	Averaged RMS Error (dB)
Linear	9.87×10^8	0	2.20×10^4	0	5.129
Nonlinear Damper Only	9.87×10^8	0	7.00×10^3	2.00×10^3	5.216
Nonlinear Spring and Damper (same damper as previous)	8.00×10^8	1.00×10^{13}	7.00×10^3	2.00×10^3	7.017
Nonlinear Spring and Damper (Optimized)	8.37×10^8	1.00×10^{13}	6.00×10^3	4.00×10^3	7.092

Finally, in Figure 4.15 the model with both nonlinear spring and damper included was tested for prediction of attenuation curves in the full load case. In adding the nonlinearity to the spring element, a wider resonant peak can be observed. Moreover, a sub-resonance is revealed again as in the idle case around 500 Hz. The sub-resonance is correctly represented for the “mi15” and “mi18” cases but goes in the opposite direction for the “mi21” case. Since the attenuation of the “mi21” case was already over-estimated with a nonlinear damper, the misinterpretation of the sub-resonance peak could possibly be a result of the damper, or at least worsened by it. Therefore a correlation between nonlinear spring element and a sub-resonance peak around 500 Hz can be concluded.

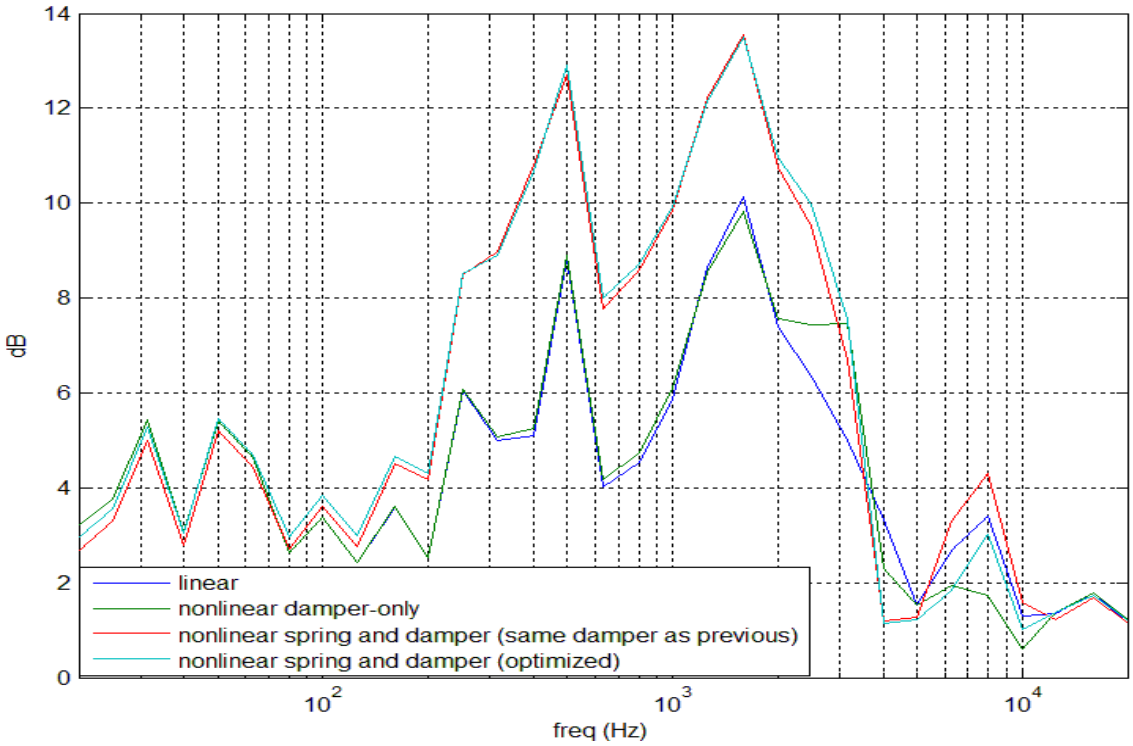

Figure 4.16. Absolute Averaged Errors between Simulated and Experimental Attenuation Curves (Full Load).

Overall, the prediction of attenuation curves at full load operating conditions, when the model itself is tuned for the idle case, doesn’t match as well with the experimental measurements as for the idle case.

Listed in Table 4.2 are the averaged root mean square errors of the simulated and experimental attenuation curves for different model parameters, while Figure 4.16 plots the absolute errors against frequencies. It can be shown that despite a better match in shapes and trends, the nonlinear models generally incur more errors. The nonlinear damper-only model is still the best choice, if not the linear one, for it not only preserves the overall accuracy but also improves accuracy in the high frequency range where attenuation is least.

In conclusion, the simplified mass-spring-damper model provides a preliminary understanding of possible nonlinearities in the engine block attenuation model and explains the corresponding dependency of the system input. The most notable dependency is the amplitude-shift of the main resonant peaks, which can be explained by an effective nonlinear damper element. A nonlinear spring was demonstrated to cause excitation of a sub-resonance at a lower frequency for some of the input cylinder pressure measurements. All these nonlinear-excited dependencies of the input are also found, in similar respects, in the experimental attenuation measurements. The model has been tested for attenuation curves generated in both operating conditions, idle speed and full load, and demonstrates that nonlinear-excited features through the simulation models are repeatable and serve as a reasonable explanation for the underlying discrepancies of the experimental measurements. Finally, limitations on the order of the linear system upon which all nonlinearities are built, and the restrictions of the degrees of nonlinearities themselves, impose fundamental limits on the overall performance of such models. Since the general trends and shapes are better matched with more nonlinearities included, a reasonable increase in complexity of the presenting models may possibly lead to a better nonlinear model that outperforms an averaged linear one, not only qualitatively, but also quantitatively.

CHAPTER 5. SOUND POWER PREDICTIONS

The attenuation curves and a mass-spring-damper-based attenuation model are intensively studied because they describe the stand-alone acoustic characteristics of the engine block and relate the noise radiation directly to readily measurable cylinder pressure. Such correlation, when calibrated properly, can serve as a powerful tool to predict the sound power of noise radiation. Measurements of noise radiation require multiple microphones and a free-field environment such as an anechoic chamber, while cylinder pressure measurements only require one pressure transducer in each cylinder. The capability of sound power prediction not only eliminates the need for sophisticated acoustic measurement procedures, but also through fast prediction provides guidelines and criteria for desirable cylinder pressure profiles in terms of the noise radiation performance. Since cylinder pressure development is directly related to the combustion process, which can be affected by injection pressure, air flow rate, injection strategies, etc. the noise level can be controlled through control of the fuel delivery and air intake, thanks to the development of modern engine management and electronic injection systems.

This chapter mainly focuses on the sound power prediction of a given set of experimental cylinder pressure measurements, first from a direct application of experimental attenuation curves, then from simulation models developed in Chapter 4. Since the corresponding acoustical measurements for the experimental cylinder pressure tested are not available, a validation of the prediction cannot be made. Instead, general behaviors and trends of prediction are studied for various nonlinearities.

5.1 Sound Power Predictions by Applying Experimental Attenuation Curves

The first set of predictions was carried out by subtracting the attenuation directly from the cylinder pressure spectrum. The same sets of cylinder pressure signals that were used as inputs to the simulations of different models in Chapter 4 were used again for sound power prediction. The cumulative sound pressure levels for the engine at idle speed and at full load are plotted in Figures 4.7 and 4.12, respectively.

The procedures for calculating sound power based on experimental attenuation curves are:

1) Analyze the cylinder pressure in the frequency domain, and generate 1/3 octave band cylinder pressure level spectra for various injection timings at different operating conditions.

2) Apply the corresponding experimental attenuation curve to the cylinder pressure level spectrum and subtract the attenuation from the pressure level. For instance, a cylinder pressure level spectrum for “mi12” at idle corresponds to an attenuation curve also for “mi12” at idle, found in Figure 4.2 as the blue curve. The differences between the two curves result in the predicted sound pressure level (A) spectrum.
3) Convert the sound pressure level (A) spectrum to cumulative sound power level (A) spectrum by first shifting the sound pressure level (A) spectrum upward (Equation (3.6)), generating the sound power level (A) spectrum and then adding the sound power levels (A) over frequencies. Note that the sound power level is in dB(A) scale and should be converted to power before addition, and the sum is later converted back to a power level in dB(A).

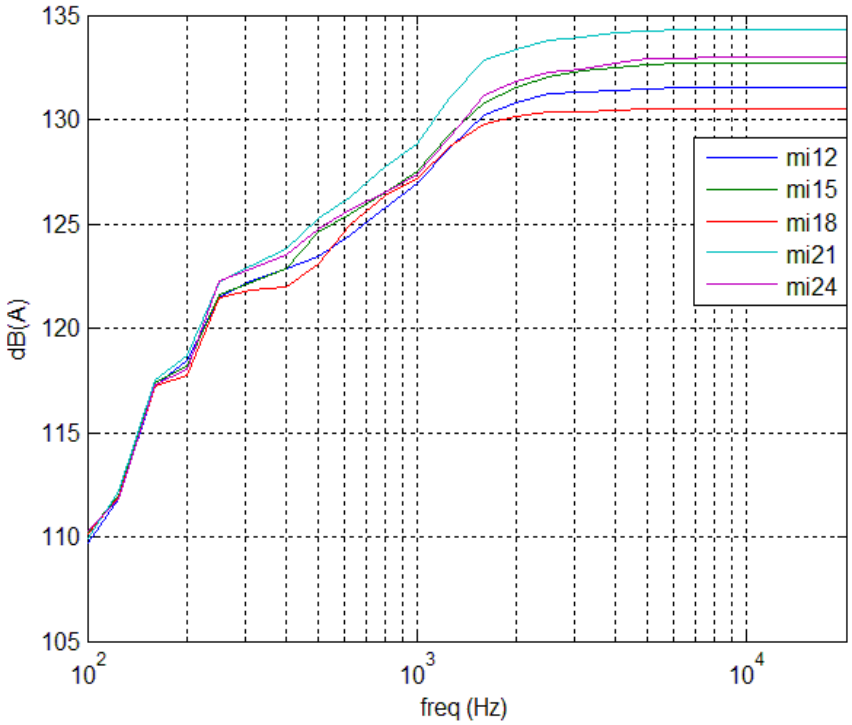

Figure 5.1. Cumulative Sound Power Level (A) Prediction through Experimental Attenuation Curves at Idle Speed.

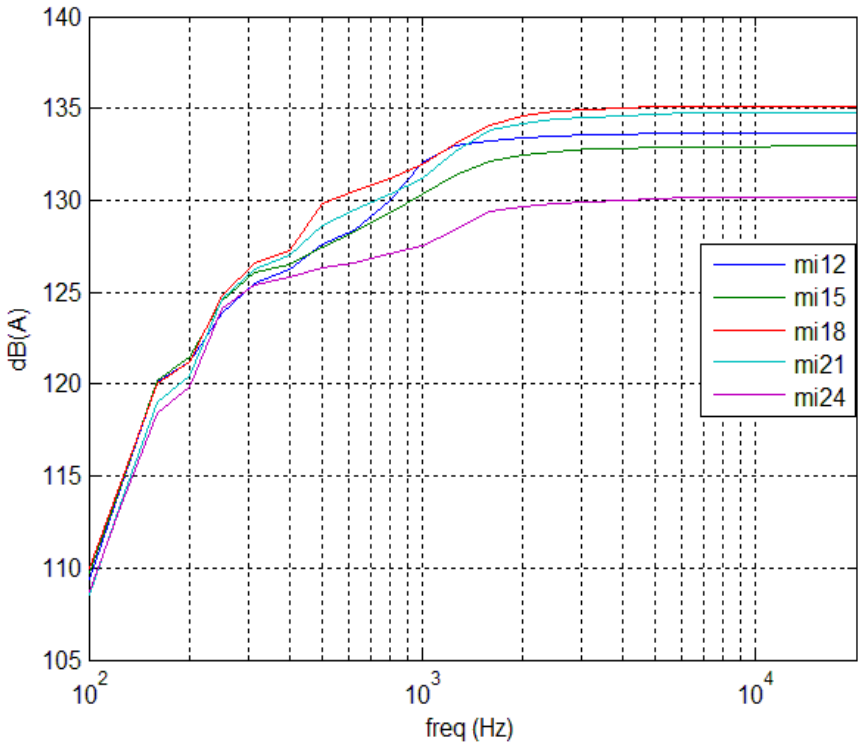

Figure 5.2. Cumulative Sound Power Level (A) Prediction through Experimental Attenuation Curves at Full Load.

The resulting cumulative sound power predictions are plotted in Figures 5.1 and 5.2, for the engine running at idle speed and at full load, respectively. Although measurements of the sound power corresponding to the cylinder pressure levels in Figures 4.7 and 4.12 are not available, qualitative evaluation of the prediction is still possible. For single-pulse injection, where there is only one major cylinder pressure peak, the noise radiation is generally in proportion to the overall cylinder pressure level. Hence, a reasonable prediction would follow the relative sequence of magnitudes of the cumulative pressure levels for different injection timings, although slight deviations are allowed. However, in both of the predictions for idle and full load conditions, by simply applying experimental attenuation, there are no evident sequences at all. The extreme cases “mi12” and “mi24”, due to their largest differences in cylinder pressure levels, should be expected to be in the right order, i.e. sound power prediction for “mi12” should be lower than that for “mi24”, while in the full load case, such sequence is completely reversed.

One explanation for these phenomena is to note that the cylinder pressures used for predictions are not the ones used for computing these specific attenuation curves in Figures 4.2 and 4.3, which have demonstrated strong dependency on the particular inputs. Comparisons of the cylinder pressure data used for sound power predictions in this research work and for calculations of the experimental attenuation curves in the previous stage of the project are included in Figures 5.3 and 5.4. Note that the absolute magnitude of the power spectrum depends on the scaling factor used for the Fast Fourier Transform (FFT). Therefore, the large

differences between averaged absolute magnitudes of the two sets of cylinder pressure spectra are partly due to different scaling factors between plots. However, relative differences between cases of various injection timings on the same plot are independent of the scaling factor, and evident differences between the two sets of cylinder pressure measurements can still be observed. The inconsistency between the two sets of data may be accounted for by potentially varying rail pressure, which was not fully regulated in closed-loop when the measurements took place, partly due to a broken rail pressure sensor.

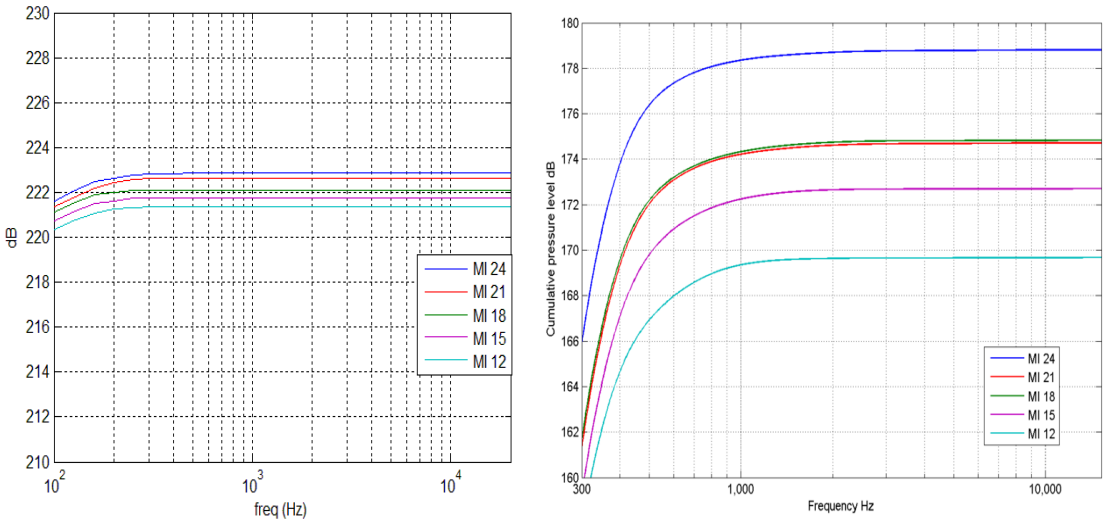

Figure 5.3. Cumulative Cylinder Pressure Used for Sound Power Predictions in This Work (left) and for Calculations of Experimental Attenuation Curves from [2] (right) (Idle Speed).

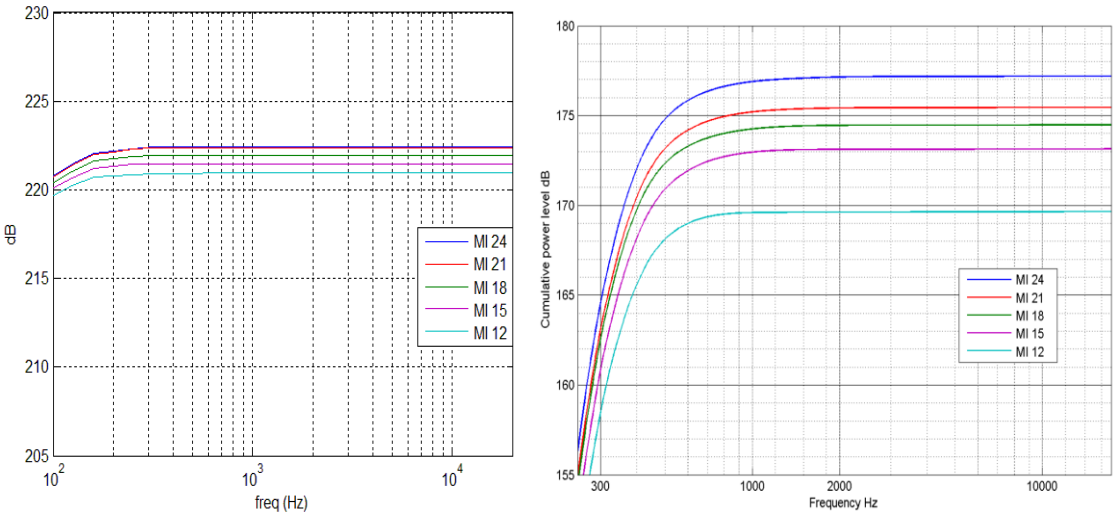

Figure 5.4. Cumulative Cylinder Pressure Used for Sound Power Predictions in This Work (left) and for Calculations of Experimental Attenuation Curves from [2] (right) (Full Load).

Another interesting point to note is that the differences between cumulative cylinder pressures used for prediction in this chapter are relatively insignificant. In fact, for both the idle and full load cases, the differences between extremes are only 2 dB, namely the highest pressure for

“mi24” is only 60% more in power density than the lowest pressure for “mi12”. Since the attenuation curves demonstrate higher attenuation for higher input cylinder pressure, it is highly possible that the predicted noise levels do not follow the same sequence as do the cylinder pressures, when the attenuation curves are not input-specific and there are only small differences among cylinder pressure levels.

The inaccuracies of prediction when directly applying attenuation curves proves the high dependency of attenuation on characteristics of the input, from a different perspective. Hence, depending on individual attenuation curves calibrated for certain sets of inputs and outputs for a more general prediction is unreliable. Discrepancies between different attenuation curves and their underlying causes need to be studied, in order to construct a more robust attenuation model for the engine block.

5.2 Sound Power Predictions by Simulation with Nonlinear Models

In an attempt to test the capability of sound power prediction of the models constructed in Chapter 4 as well as to understand the possible impact of nonlinearities on predictions, the simulated outputs from the mass-spring-damper-based models, representing sound pressure measurements, are further processed to generate the sound power level. The detailed steps for using a SIMULINK model for sound power predictions are:

1) Feed in cylinder pressure measurements for sound power predictions directly into the model, run the simulation and record the simulated sound pressure outputs.
2) Analyze the sound pressure data in the frequency domain, generating the sound pressure level (A) spectrum with an A-weighting filter.
3) Same as Step 3 in Section 5.1, convert the sound pressure level (A) spectrum to sound power level (A) spectrum first then compute the cumulative sound power level (A) spectrum.

Models with the same parameters studied in Chapter 4 (Table 4.1) are tested for predictions, namely the linear model, the nonlinear damper-only model and the nonlinear spring and damper (optimized) model. The nonlinear spring and damper model with the same damper as in the nonlinear damper-only model was not studied for prediction and thus the optimized nonlinear spring and damper model is simply referred to as the nonlinear spring and damper model. The same cylinder pressure inputs as used in the previous prediction applying experimental attenuation curves directly were used for the mass-spring-damper-model-based sound power prediction, the results of which are plotted in Figures 5.5 to 5.10.

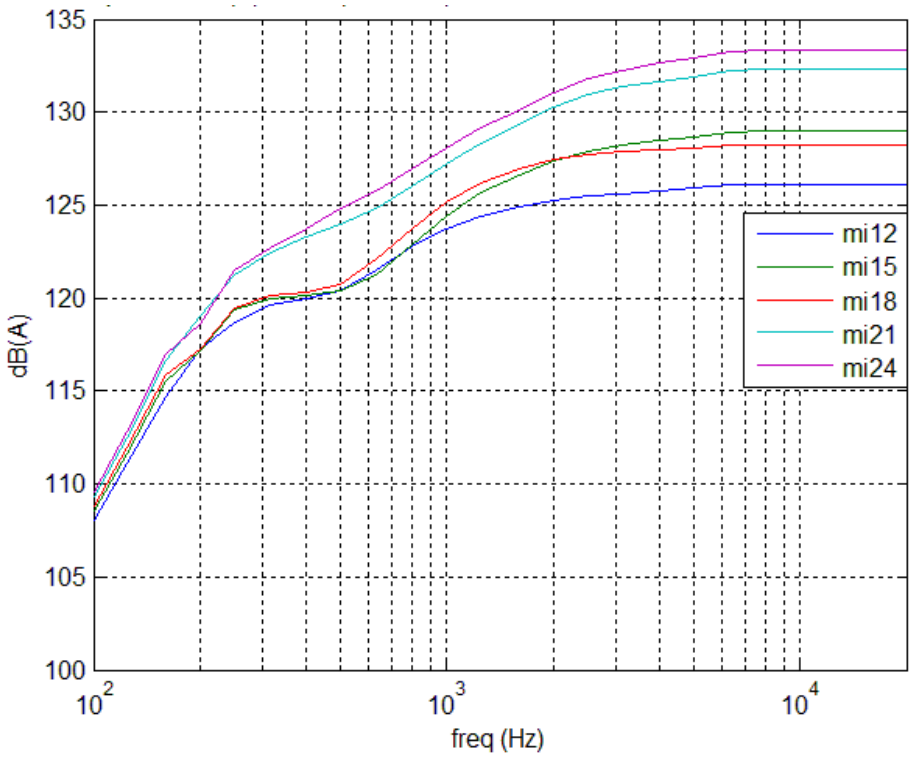

Figure 5.5. Cumulative Sound Power Level Prediction by a Linear Model (Idle Speed).

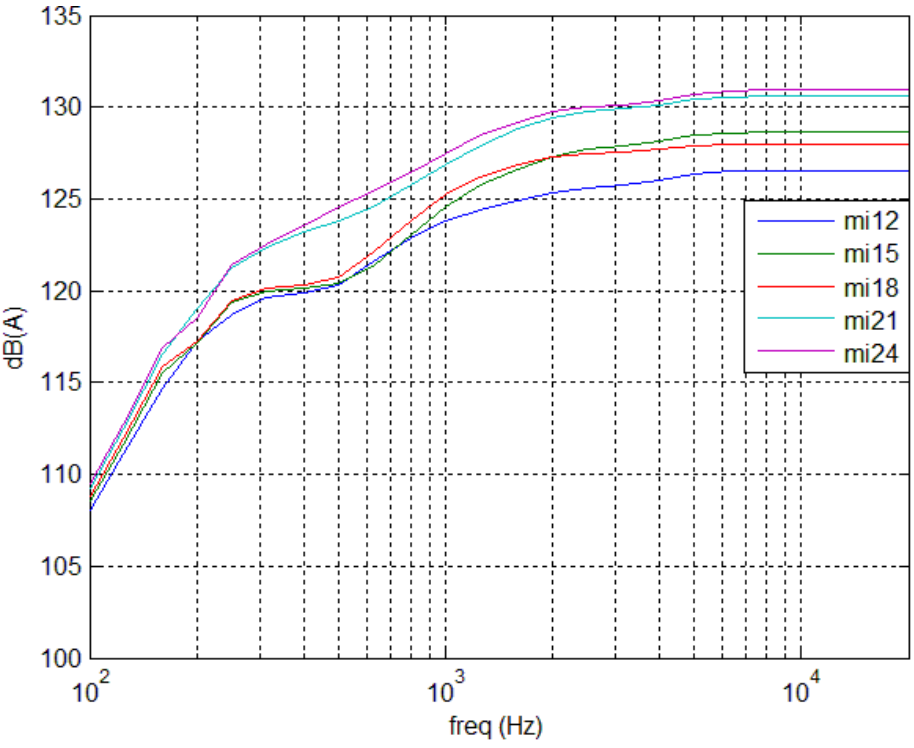

Figure 5.6. Cumulative Sound Power Level Prediction by a Nonlinear Damper-Only Model (Idle Speed).

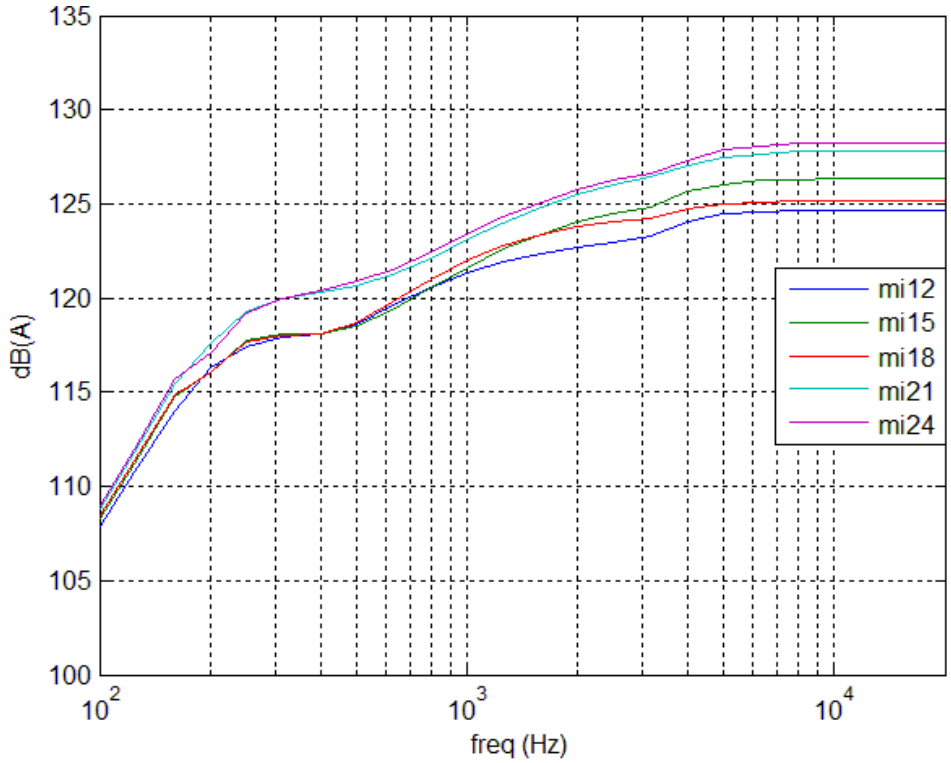

Figure 5.7. Cumulative Sound Power Level Prediction by a Nonlinear Spring and Damper Model (Idle Speed).

Figures 5.5 to 5.7 show the cumulative sound power prediction for the engine running at idle speed by various models. The predictions in general, in terms of the supposed sequence of the relative cumulative sound power levels, are fairly good. All of the three models, the purely linear, the nonlinear damper-only, and the nonlinear spring and damper, give the same prediction of sequence of powers, which generally follows the sequence of corresponding cylinder pressure levels except for the “mi15” and “mi18” cases. However, due to the small differences between cylinder pressure levels, such interchange is possible. The introduction of a nonlinear damper, as opposed to a purely linear system in Figure 5.5, demonstrates the feature of amplitude shift, namely the larger the cylinder pressure input, the greater the corresponding attenuation will be over high frequency ranges. As a result, prediction of sound power level in Figure 5.6 not only sees an overall reduction of sound power level compared to prediction from a purely linear model, but also a reduction in relative differences between predictions for various injection timings. Further increase in nonlinearities by including both nonlinear spring and nonlinear damper (Figure 5.7) continues to reduce the overall sound power level and also changes the relative differences between different predictions for various injection timings.

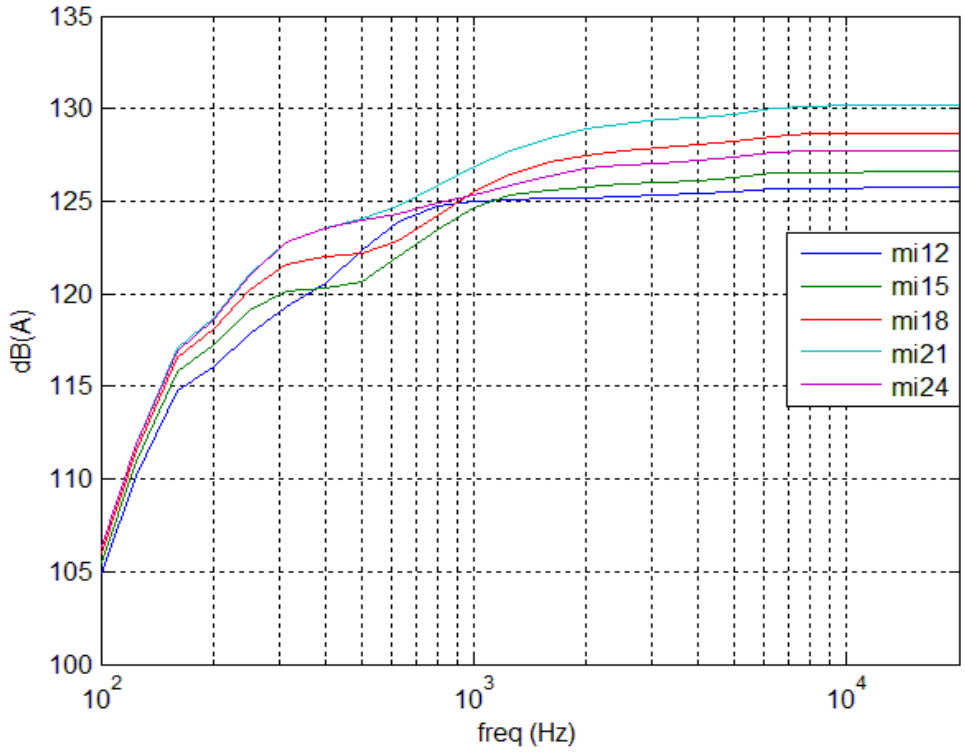

Figure 5.8. Cumulative Sound Power Level Prediction by a Linear Model (Full Load).

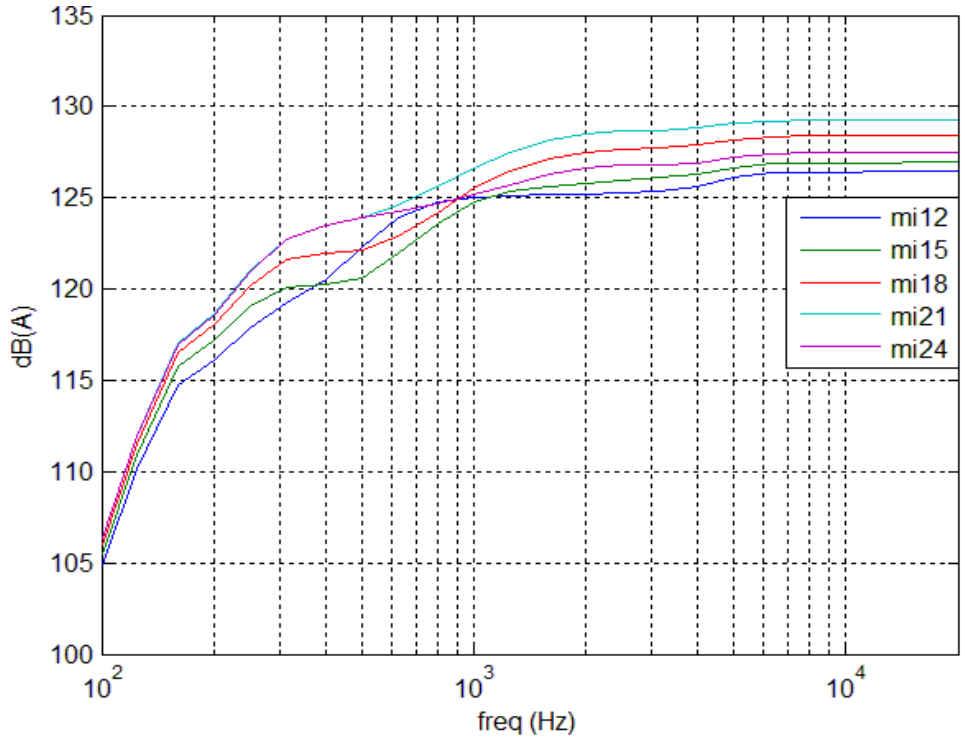

Figure 5.9. Cumulative Sound Power Level Prediction by a Nonlinear Damper-Only Model (Full Load).

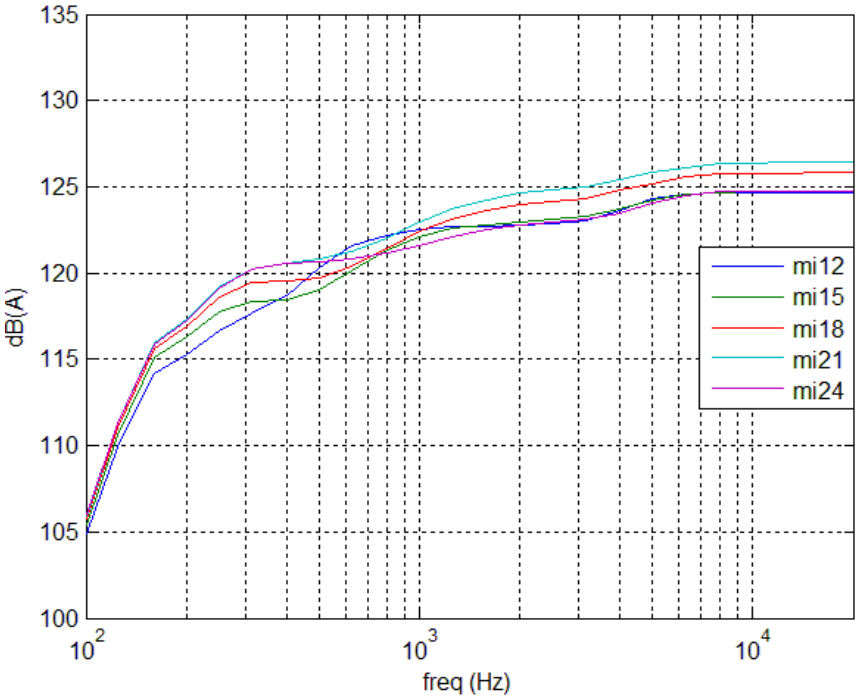

Figure 5.10. Cumulative Sound Power Level Prediction by a Nonlinear Spring and Damper Model (Full Load).

Figures 5.8 to 5.10 show the cumulative sound power level predictions for the engine running at full load with the same models as previously for predictions for the engine running at idle speed. Similar conclusions to those in the idle case can be drawn for the full load case.

First, the relative sequence of predictions in terms of different injection timings generally follows the expected order, i.e., in accordance with the cylinder pressure levels. One exception is for the “mi24” case, where the supposedly highest sound power levels fall in between with the other cases, but still no lower than the “mi12” case, representing the supposedly lowest sound power levels. Secondly, adding nonlinearities in general increases the overall attenuation and leads to reduced sound power predictions. Besides, a nonlinear damper accounts for the amplitude-shift feature of the attenuation and reduces the relative differences between sound power predictions among cases with various injection timings. Further including a nonlinear spring, as stated in Chapter 4, increases the modeling errors and leads to more uncertainties in the sound power prediction results.

In conclusion, the sound power predictions with mass-spring-damper-based models with or without nonlinearities generally outperform those computed by directly applying the experimental attenuation curves, calibrated for a different set of measurements. The advantages of simulation-model-based predictions over attenuation-curves-based predictions are that the models are based on a physical mass-spring-damper system, which resembles the vibrating engine block, and aim at capturing the underlying acoustic characteristics, linear or nonlinear, of the engine block, as opposed to running calibrations case by case. However the

accuracies of predictions with different simulation models cannot be verified at the moment due to lack of reliable experimental data.

CHAPTER 6. CONCLUSIONS

6.1 Summary of Contributions

The research undertaken has successfully identified nonlinearities in the noise attenuation system for a diesel engine block. The nonlinearities include, but are not limited to, both nonlinear stiffness and nonlinear damping of the engine block. In the phase of the exploration of nonlinearities, a mass-spring-damper-based model was developed as opposed to the conventional attenuation-curve-based model, where a linear assumption is necessary but questionable. Through simulation of several nonlinear mass-spring-damper models and comparisons with the experimentally-determined attenuation-curve-based models, similarities were noted and attributed to a result of the two major sources of nonlinearities, nonlinear spring element and nonlinear damper element.

The research interest in nonlinearities started from dependency of the experimentally-determined attenuation curves on injection parameters. Instead of being a consistent overlapped curve for different test cases, featuring different combustion processes, significant discrepancies were noticed and demonstrated nonlinear behaviors such as amplitude-shift of the resonant peaks and occasional occurrences of sub-resonances. Consequently a model that has the freedom to implement nonlinearities and test for their existence was sought, and finally a mass-spring-damper-based physical system was chosen. At first, the system was set linear and tuned to match with the averaged attenuation curves determined experimentally. Later, nonlinear spring and nonlinear damper were introduced, and the nonlinear behaviors were observed in the simulated attenuation curves.

Furthermore, an attempt to predict sound power radiation with only cylinder pressure measurements was performed for both the attenuation-curves-based and the mass-spring-damper-based model. The reliability of predictions was roughly analyzed based on the expected order of sound power predictions for cases with different injection timings. The impact of nonlinearities on trends of predictions was also discussed and expected validation through future experiments.

6.2 Summary of Results

Simulation with nonlinearities in the attenuation model suggested that the amplitude-shift of the resonant peaks of attenuation curves, representing cases of different injection timings, can be accounted for by a nonlinear damper while the occurrences of sub-resonances for several test cases are closely related to a nonlinear spring. The bandwidths of the main resonant peaks were also increased by incorporation of a nonlinear spring, and relatively flat resonant peaks were observed in the experimental attenuation curves as well. Hence, a correlation between inherent nonlinear spring and damper elements, and nonlinear behaviors of the engine block attenuation system, was concluded.

With the limit on the order of the simulation system and the degrees of the inherent nonlinearities studied, an averaged linear model was still the preferred choice in terms of least root mean square errors to the attenuation curves computed from experimental measurements. The best nonlinear model is a nonlinear damper-only model, which has the same overall accuracy as the linear model but better performance over high frequency ranges. A model with nonlinear spring further incorporated generally increases the overall errors, although it better explains several nonlinear behaviors of the engine block, as discussed previously. It is possible, with increased order of the system model and degrees of nonlinearities, that the best overall accuracy is achieved when both nonlinear spring and damper elements are present. The models developed were all first tuned to least error with the experimental data measured when the engine is at idle. Validation with prediction of attenuation curves when the engine is at full load were then carried out, and comparisons with the experimental measurements indicated the models generated were reliable.

Lastly, the results from predictions of sound powers suggested that the model developed in this thesis, namely the mass-spring-damper-based model, is more robust than the input-sensitive attenuation-curves-based model. Further analyses of impact of nonlinearities on predictions showed that the differences between predicted sound power levels of various cases, in terms of injection timings, tend to decrease as the degree of nonlinearities increases. However, the model that made the best sound power predictions could not be justified until further acoustic measurements are made available.

6.3 Recommendations for Future Work

As mentioned in the summary, several questions remained to be answered in an attempt to understand the nonlinearities and generate a robust model for accurate sound power predictions. These questions include the accuracy of prediction of the current model, other potential nonlinearities included, etc. Primarily, the recommendations for future work include:

1) Conduct more measurements of both cylinder pressure and corresponding sound pressure measured via microphones, for different combustion processes. Besides the obvious reason to justify sound power predictions, such measurements should also focus on answering two questions. The first question is whether the nonlinear behavior observed and analyzed among attenuation curves in this thesis is repeatable. An important notion is that cylinder

pressure measurements for single pulse injection generally become insignificant and result in poor signal-to-noise ratio over 300 Hz (Figures 4.7 and 4.12). Large discrepancies between experimental attenuation curves observed and analyzed in this study also fall in the range of high frequencies. In 2008, another group of researchers at Herrick Laboratories also noticed discrepancies of attenuation curves for different operating conditions over high frequency range, which were later identified as a result of cylinder pressure signals comparable in magnitude with the noise floor [19]. Therefore, repeatability of the highly input-correlated trends of discrepancies, namely amplitude shift of resonant peaks and sub-resonances for some of the cases, needs to be examined to exclude the possibility of pure impact of measurement noise. The second question is whether the mass-spring-damper-based model generated in this thesis can be validated in a multi-pulse injection scenario, and if not, what other nonlinearities need to be further included in the model.

2) Tune and validate the attenuation model based on quality of sound power predictions, instead of matching with experimental attenuation curves. Since accurate sound power predictions are of most interest, it will be natural to compare the predictions and use this error as an indicator of the validity of a model.
3) Develop automated-tuning algorithms to find the combinations of model parameters for best performance. The tuning of the model in this thesis was based on trial-and-error to reach the least possible root mean square errors. This technique, however, cannot guarantee a fast and effective tuning of parameters especially when the degrees of nonlinearities increase. Automatic tuning is needed to ensure the model can self-adjust to a large number of experimental measurements and compute the optimized sets of parameters for different engines.
4) Study the attenuation model with other nonlinear modeling techniques. The current modeling is based on a physical vibrating system, which has limitations in revealing complicated correlations between input and output. Other popular modeling techniques, such as artificial neural networks, may be an alternative. With proper settings of parameters such as number of nodes and layers, specific computing algorithms, the relationship between cylinder pressure and noise power may be readily learned and a reasonable prediction can be expected.
5) Understand the physical sources of nonlinearities in the engine block. So far, the engine block was studied only based on input and output data from the attenuation system, and the model proposed is purely data-driven. However, to better understand the noise attenuation, the physical nature of nonlinear behavior of the engine block needs to be analyzed.

LIST OF REFERENCES

LIST OF REFERENCES

[1] Sasidharan, P. May 2008. Development of an Electronic Fuel Injection System for a Small Electric Power Unit. M.S. thesis, Purdue University.

[2] Bhat, C. May 2010. Influence of Electronic Fuel Injection Parameters on Combustion-induced Noise in a Small Diesel Engine. M.S. thesis, Purdue University.

[3] Yang, M. and Sorenson, S. 1994. Survey of the Electronic Injection and Control of Diesel Engines. SAE paper 940378.

[4] Aaberg, D. Generator Set Noise Solutions: Controlling Unwanted Noise from On-site Power Systems. Technical information from Cummins Power Generation Inc. Power topic 7015.

[5] Jenkins, S. 1975. Analysis and Treatment of Diesel-Engine Noise. Journal of Sound and Vibration (1975) 43(2), 293-304.

[6] Austen, A. 1958. Origins of Diesel Engine Noise. Institution of Mechanical Engineers, London, October 24, 1958.

[7] Ricardo, H. 1931. The High Speed Internal Combustion Engine. First edition, Blackie & Sons Ltd., Glasgow.

[8] Ricardo, H. 1968. Memories and Machines. The Pattern of my Life. Constable & Co. Ltd.

[9] Priede, T. 1980. In Search of Origins of Engine Noise – an Historical Review. SAE paper 800534.

[10] Withrow, L. and Fry, A. 1944. Physical Characteristics of Roughness in Internal Combustion Engines. SAE Journal, 52, p.100.

[11] Fry, A., Stone, J. and Withrow. L. 1947. Analysis of a Shock-Excited Transient Vibration Associated with Combustion Roughness. SAE Quarterly Transactions, 1, p.164.

[12] Priede, T. 1956. The Origins of Diesel Engine Noise. CAV Ltd., Report No. C. 29147.

[13] Austen, A. and Priede, T. 1958. Origins of Diesel Engine Noise. Symposium on Engine Noise and Noise Suppression. The Inst. Mech. Engrs, London.

[14] Anderton, D. 1979. Relation between Combustion System and Engine Noise. SAE paper 790270.

[15] Desantes, J. 2001. Wavelet Transform Applied to Combustion Noise Analysis in High-Speed DI Diesel Engines. Proceedings of the 2001 Noise and Vibration Conference. NOISE2001CD.

[16] Priede, T. 1960. Relation between Form of Cylinder Pressure Diagram and Noise in Diesel Engines. Proc. Inst. Mech. Engrs (A.D) p.63.

[17] Diesel Engine Management, Fourth Edition. 2005. Robert Bosch GmbH.

[18] American National Standards Specification for Sound Level Meters, ANSI S1.4-1983.

[19] Lee, M., Bolton, J.S. and Suh, S. 2008. Estimation of the Combustion-Related Noise Transfer Matrix of a Multi-Cylinder Diesel Engine. Meas. Sci. Technol. 20 (2009) 015106 (13pp).